TERMINUS DYNAMICS AND DEFORMATION OF PROGLACIAL SEDIMENTS AT THE ADVANCING TAKU GLACIER, ALASKA, U.S.A.

By

Elsbeth Maria Kuriger

RECOMMENDED:

Advisory Committee Chair

Chair, Department of Geology and Geophysics

APPROVED:

Dean, College of Natural Science and Mathematics

Dean of the Graduate School

August 1, 2005

Date

TERMINUS DYNAMICS AND DEFORMATION OF PROGLACIAL SEDIMENTS AT THE ADVANCING TAKU GLACIER, ALASKA, U.S.A.

A

THESIS

Presented to the Faculty

of the University of Alaska Fairbanks

in Partial Fulfillment of the Requirements

for the Degree of

MASTER OF SCIENCE

By

Elsbeth Maria Kuriger, Diploma in Natural Sciences

Fairbanks, Alaska

August 2005

Abstract

Taku Glacier has advanced about 7 km since 1890. The continuing advance is the result of the tidewater-glacier cycle. In the last several decades, the glacier has bulldozed a berm of marine and fluvial sediments from the fjord bottom and produced so-called push moraines. The mobilization of these sediments, which were locally lifted more than 20 m above sea level by 2004, has happened episodically rather than steadily. The last major proglacial sediment deformation was observed in 2001. Since then, most deformation has been localized within some meters of the terminus. Between 2002 and 2004 surface velocities and displacements were measured across the terminus and in the proglacial area. The displacement were highest between March and June and decreased with distance from the terminus. The sediments were presumably deforming internally rather than moving along a basal décollement. A simple model and sensitivity analysis show that major movement along this layer will most likely happen if (1) the glacier steepens its surface topography, (2) the proglacial sediment wedge shortens and steepens its surface slope or (3) the water pressure increases in order to reduce the frictional resistance.

Table of Contents

List of Figures

List of Tables

List of Other Materials

List of Appendices

Acknowledgements

First I would like to thank all the people responsible for giving me the opportunity to work in an interesting research field and at an exciting study site. Roman Motyka, the main initiator of the Taku project, supported the idea of combining glaciology and geology, a combination that suited my interests very well. His hospitality including the foreign movie nights are highly appreciated. A deep thanks goes to my advisor Martin Truffer. I never had the feeling of having a dominant boss, he was more a good friend even during scientific discussions. Only his strange language caused misunderstandings and an interpreter would have been helpful. Keith Echelmeyer and Lewis Shapiro served on my advisory committee and offered many suggestions during the preparation of the manuscript. The same is true for Will Harrison and mit Gottes Hilfe möge er noch lange gut erhalten bleiben.

My work would not have been possible without all the field assistants. I want to thank Adam Bucki for his willingness to learn my swiss swearing techniques, Ellie Boyce for not making me eat beef ravioli for breakfast, Jason Amundson for eating my band-aid and for not getting up at 6 am. Tinu Lüthi and Shad O'Neel also helped during fieldwork.

Contributions to my research were made by Jeff Freymueller, Dennis Trabant, Rod March, Kenji Yoshikawa, Chris Larsen, By Valentine, Sandy Zirnheld and all the people in the Glaciology Lab. Special thanks go to Anthony Arendt who provided many climate data and – much more important – swiss chocolate!

The whole study time in Alaska would not have been possible without Robin Wilson and his family, who made the daily life in the woods of Fairbanks an unforgettable experience. I want to thank Tanja, Anja, Eamon, Heike, Dana, Sébastien, Amanda, Susan, Ann, Inari, Leslie and many others for the time we spent together other than work.

My deepest thank goes to Tinu. He did not think that I was crazy to apply for grad school at UAF (maybe I was?) and shared the adventure "Alaska" with me. My dream of coming to Alaska for more than just vacation would not have been fulfilled without his support.

Chapter 1
General Introduction

An advancing glacier can – under certain conditions – produce so-called "push moraines", glaciotectonic moraines just below or in front of the terminus. The formation of push moraines contains information about the interaction between the glacier and its foreland. The conditions under which they form, move or are reactivated after a period of standstill are not fully understood. The advancing Taku Glacier offers a rare opportunity to study an actively deforming glacier terminus and its foreland.

The main chapter of this thesis deals with an important aspect of the glacier-sediment system: How does an advancing ice front interact with its foreland? It has been prepared for submission to the Journal of Geophysical Research JGR (Earth Surface). Roman Motyka, Martin Truffer and Adam Bucki will be co-authors on the paper.

Appendices included in the thesis contain information that did not fit into the paper. The first appendix is a sample of various pictures along the terminus of Taku Glacier and its foreland. It mainly shows a variety of deformational features observed in 2003 and 2004. Appendix B shows the results from radio-echo soundings in the terminal area of Taku Glacier. All data files from this and the following appendices are also included on the data CD in the pocket at the end of the thesis. Nevertheless, a printed version of the most important data is useful, since the CD might get lost or the compatibility of data formats or CDs with future computers and software might change. Appendices C to E include the results from different GPS surveys on the glacier and sediments between 2002 and 2004. In 2004, ice and water samples were taken in order to determine the existence of freeze-on layers at the glacier bed. These results are presented in Appendix F. Appendix G gives a list of files available on the attached data CD.

Chapter 2
Episodic Reactivation of Large Scale Push Moraines in Front of the Advancing Taku Glacier, Alaska, U.S.A[1]

Abstract

Taku Glacier, an advancing former tidewater glacier in Alaska, has actively been pushing its proglacial sediments along part of its terminus over the last fifty years, producing so-called push moraines. The mobilization of these sediments, which were locally lifted more than 20 m above sea level by 2004, has happened episodically rather than steadily. The last major event of proglacial sediment deformation occurred in 2001, presumably caused by sliding along a basal detachment layer. Since then, most deformation has been localized within a few meters of the terminus, including impressive deformational features of the terminal ice, where slabs of ice, tens of centimeters in thickness, have undercut proglacial vegetation and lifted it up. Between 2002 and 2004 surface velocities and horizontal displacements were measured across the terminus and in the proglacial push moraine area. Sediment displacement was highest between the end of March and mid-June. A decrease in displacement with distance from the terminus revealed that the sediments were deforming internally rather than along a basal décollement. We present a simple model which suggests that, under 2004 conditions, reactivation of major movement along this layer is unlikely to happen, unless some critical factors change. These factors include (1) a steepening of the glacier surface, (2) an increased surface angle of the sediment wedge and/or (3) higher water pressure in the system, which decreases the effective frictional resistance. An observed wet clay-rich layer presumably acted as a major fault plane during the 2001 event.

[1]This chapter will be submitted to the Journal of Geophysical Research JGR

2.1 Introduction

An advancing glacier can – under certain conditions – produce so-called "push moraines", which are glaciotectonic moraines just below or in front of the glacier terminus. Push moraines display a wide range of different morphologies, at scales from a few meters at the glacier terminus to several hundred meters beyond the advancing ice front. The conditions under which they form are not fully understood and neither are the conditions for continuation or reactivation of push moraine development. This paper deals with an important aspect of the interaction between an advancing glacier and its foreland that has rarely been investigated: to determine the conditions under which a glacier pushes and reactivates existing large-scale deformational bulges in front of its terminus, rather than overriding them.

Glaciotectonic processes are a significant part of a glacier system. *Bennett* [2001] reviewed numerous detailed geomorphological studies of push moraines from different glaciers in various locations. Most of these studies described ice-marginal sediment deformation [*Humlum*, 1985; *Krüger*, 1985] as well as multi-crested push moraines, which extended several hundred meters beyond the glacier terminus [*Croot*, 1987; *Boulton et al.*, 1999]. *Sharp* [1984] and *Krüger* [1993] described deformation at the glacier-sediment interface, which involved both ice and sediments. The only quantitative and very comprehensive study of active push moraines was published by *Kälin* [1971]. The advance of Taku Glacier offers a rare opportunity to collect data on an actively deforming glacier terminus and its foreland.

Push moraines, such as those at Taku Glacier, are mechanically analogous to wedges of soil or snow pushed by a moving bulldozer. A simple model of the process was presented by *Davis et al.* [1983] and *Dahlen* [1984] who used it to examine the deformation of accretionary wedges and propagation of thrust faults on tectonic scales. The resulting "critical taper theory" links the force balance of a sediment pile to its bulk geometry and mechanical properties and to the kinematics of its deformation. *Van der Wateren* [1995] and *Fischer and Powell* [1998] applied the critical taper theory to ice-pushed proglacial moraines. Unlike a bulldozer, a glacier is compliant and adapts its shape while pushing the sediments beyond the advancing terminus. On a much smaller scale, sandbox experiments reproduced many of the features observed on tectonic scales [e.g., *Mulugeta and Koyi*, 1992; *Lohrmann et al.*, 2003]. Taku Glacier provides a natural laboratory on a larger scale than sandbox

experiments and the development of push moraines can be studied within a reasonable time period.

The main research question addressed in this paper is how an advancing ice front interacts with its foreland. Specifically, we investigate why large-scale deformation occurs episodically rather than continuously, and under what conditions this major deformation can be reactivated. In order to answer these questions, we will (1) present a variety of observations of small-scale deformation along the terminus (Section 2.3). Many of these observations have not been previously reported. (2) We present our measurements in the proglacial area (Section 2.4) and (3) use these measurements along with the critical taper theory to explain the episodic deformation of the sediment wedge and to find necessary conditions for future reactivation of large-scale deformation (Section 2.5).

2.2 Background on Taku Push Moraines

Taku Glacier (700 km^2, 60 km in length) , a temperate, maritime glacier draining the Juneau Icefield, has advanced about 7 km since 1890 into the north end of Taku Inlet (Figure 2.1) after more than a century of calving retreat [*Motyka and Begét*, 1996]. The present dynamics of Taku Glacier are the result of the tidewater-glacier cycle [*Meier and Post*, 1987] and a large accumulation to total area ratio (AAR) of about 0.90 during the last century [*Post and Motyka*, 1995]. Taku Glacier had a calving ice-front along its entire terminus until 1948, when the shoal terminal moraine was raised above sea level in the central part of the terminus. During subsequent years, ice-proximal moraines developed along most of the face with a dominant deformational push moraine complex in the center. Comparison of aerial photographs from different years has shown that this broad area of proglacial deformation has remained at the same relative position with respect to the terminus since its first appearance in 1948. The development of these moraines plays an important role in the advance of the glacier, as they protect the ice from warm ocean water and thereby prevent ice loss due to calving and submarine melting. The sediment sources for the moraines are primarily remobilized subglacial sediments with additional fluvial contributions from Taku River. Radio-echo soundings from 2003 and 2004 (Appendix B) show that the glacier bed forms a trough upglacier of the push moraine complex with a depth of 120 m below sea level at the location of the 1948 shoal moraine. Comparisons with depth soundings by *Nolan*

et al. [1995] have shown sediment excavation of $3.7 \pm 0.8\,\mathrm{m\,a^{-1}}$ between 1989 and 2004 along the centerline of the glacier [*Motyka et al.*, 2005].

A series of aerial photographs taken between 1979 and 1996 revealed an episodic change in shape of the shoal proglacial area. The existence of multiple deformational bulges in the middle part of the terminus was clearly visible by 1979 [*NASA*, 1979]. Their shape changed noticeably by 1989 [*U. S. National Ocean Service*, 1989] but remained more or less constant over the subsequent years [*U.S.D.A. Forest Service*, 1996]. In 2001, large-scale sediment deformation was observed and three main bulges (bulge 1 to bulge 3 in Figure 2.2) and several smaller ones formed up to 200 m in front of the terminus [*Motyka and Echelmeyer*, 2003]. They advanced at an average rate of $9 - 15\,\mathrm{cm\,d^{-1}}$ during the summer. This large movement slowed down by orders of magnitude or ceased completely by September 2001 despite the ongoing terminus advance. Since then, most deformation has occurred within a 5-m-wide section of the terminus or the ice has simply overridden its terminal moraines. Hence, movement on three different scales has coexisted since 2001.

In this paper we use the term 'ice-proximal ridges' for the ice-proximal moraines, which are $1 - 5\,\mathrm{m}$ high sediment piles within 5 m of the terminus. 'Proglacial bulges' or just 'bulges' refer to the large-scale deformational features up to 200 m beyond the terminus. For the general term 'push moraine' we use the definition by *Bennett* [2001]. All values for elevation are presented in height above ellipsoid (HAE) which is about 4.1 m higher than geoid height (Geoid99) in our study area.

2.3 Deformation at the Glacier-Sediment Interface

Ice-proximal ridges were observed during the period of large scale deformation in summer 2001 [*Motyka and Echelmeyer*, 2003]. They increased in size and/or changed their deformational style by 2004. In addition to the sediments, glacier ice at the very terminus also became incorporated into the deformation. In this section we describe features at five locations (A, B, C, D, E, Figure 2.2a). They have different characteristics, even though they are only a few hundred meters apart. Descriptions are based on photographs and observations taken in June and August 2003 and 2004. We also present velocity measurements across the ice-proximal ridge at site E. We used precision GPS receivers (TRIMBLE 4000 and TRIMBLE 5700) for position measurements and processed the baselines against a fixed

base station situated 100 m in front of bulge 1. The horizontal error in baseline length is about 6 mm.

Site A is located about 400 m west of the area of the proglacial bulges. A roughly 6-m-high and 100-m-long ice-proximal ridge was the dominant feature (Figure 2.3a). It has caused the advancing glacier to form several $2 - 3$ m thick imbricate thrusts with steep upglacier dipping angles. The glacier outwash in front of the ridge was at an elevation of about 10 m (HAE) and did not show any signs of deformation. This feature was very localized and could not be observed anywhere else along the terminus. The ridge itself was composed of unsorted, well rounded cobbles and boulders, presumably englacially or subglacially remobilized fluvial outwash.

Site B is situated at the very western end of the push moraine area at an elevation of 15 m (HAE). Between 2002 and 2004 the terminus advanced 29 m without any noteworthy deformation of a small secondary bulge (Figure 2.3b). The advancing glacier was about to override a 1-m-high sediment ridge.

Site C is in an area where the deformation of 2001 raised the proglacial area from about 10 m to 21 m (HAE). The glacier advanced about 28 m between 2002 and 2004. In 2003 and 2004 glacial runoff was abundant and distributed through the area and was flowing either along the terminus or along the toes of small secondary bulges close to the terminus. There were few ice-proximal ridges in this area and none was higher than 0.5 m. We observed that individual ice layers peeled off the under- or overlying ice. Figure 2.3c shows a sliver of ice about 10-cm-thick that formed a single fold with its axis parallel to the terminus. The lower limb was connected to the glacier, the upper limb was rotated back toward the glacier. We found ice covered by water in front of and below the fold.

Site D, at an elevation of 26 m (HAE), is at a location where an approximately 4-m-deep and 10-m-wide depression separated the push moraine area from the glacier terminus in spring 2003. This depression, located at the eastern end of the area, served as a major water outflow channel from the glacier. The glacier advanced 15 m between 2002 and 2004. By spring 2004 the depression was completely ice-filled and sediment ridges, up to 2.5-m-high, had formed in front of the terminus and were about to be overridden by the advancing ice (Figure 2.3d). 1-m-thick ice slabs of mainly clear dark ice had been pushed over the pile of sediments. A survey marker close to the edge of the glacier moved at a horizontal

ice velocity of about $17\,\mathrm{cm\,d^{-1}}$ and a vertical upward velocity of about $1\,\mathrm{cm\,d^{-1}}$. Within a few meters upglacier from the terminus, the glacier surface became steep and difficult to access.

Site E was characterized by a consistent style but increasing intensity of deformation between 2003 and 2004 (Figure 2.4). In June 2003 we detected recently torn and uplifted vegetation on a 0.5-m-high sediment ridge. The ridge was ice-cored with an about 3-cm-thick slab of ice which was connected to the glacier ice (Figure 2.4a). Ridges undercut by advancing ice slabs were common along a 100-m-long section around this site. The sediments of the ridge were a composite till (remobilized glacier outwash, subglacial till) without any internal structure. They were composed of boulders and cobbles in sand, silt and clay. In June 2004 the height of the sediment ridge was about 2 m, significantly more than in June 2003. A slab of ice had been pushed up along the ice-proximal part of the ridge (Figure 2.4b). The mean thickness of this dark clear bubble-free ice was 0.5 m at the slab itself and 0.65 m at the hinge which connected the slab to the glacier at a 90° angle. The ice slab was inclined at a 40° angle at its base and was almost vertical at the top. We measured a mean dip angle of the glacier surface of 35°, which became almost 70° 7 m behind the terminus and decreased to a mean angle of about 17° further upglacier. During steam-drilling for survey markers we hit a 60-cm-thick cavity 5 m behind the terminus where the vertical ice thickness reached 3 m (Figure 2.4c). A few meters to the side, a thrust fault had developed within the ice, and no vertical or folded ice slabs were observed (Figure 2.4b). This emphasizes the variability of sediment and ice deformation within short distances of the terminus.

We placed six survey markers across the proximal ridge at site E, from the glacier ice to the intact vegetation (points 1 to 6 in Figure 2.4c). Points 1 to 3 were measured over a four-day interval, point 4 on top of the ice slab twice within 24 hours. The high ablation rate of 10 to $15\,\mathrm{cm\,d^{-1}}$ made more extended measurements of that point difficult. Markers 5 and 6 in front of the sediment pile were surveyed over a 20-day period. Figure 2.4c summarizes the results. Most of the horizontal compression occurred within three meters across the sediment ridge (between points 3 and 5), during which the ice between points 1 and 3 was moving as a single block. The vertical upward movement at the top of the ice slab (point 4) was $13.5\,\mathrm{cm\,d^{-1}}$, similar to the ablation rate at this location. Point 6 did not show any

movement on this scale. Between June and August 2004 the crest of the ridge propagated at about $6\,\mathrm{cm\,d^{-1}}$. Our observations between 2003 and 2004 revealed that underthrusting of the ridge by the advancing ice and subsequent mass wasting at the front of the ridge was the general process of moving the ridge forward rather than bulldozing. Site E was at an elevation of 25 m (HAE) and advanced 24 m between 2002 and 2004.

2.4 Deformation in the Proglacial Area

2.4.1 Movement of the Proglacial Bulges

Major movement of the bulges (on the order of $\mathrm{cm\,d^{-1}}$) ceased by fall 2001 [*Motyka and Echelmeyer*, 2003]. To monitor potential reactivation of movement, we established survey markers along profile P-P' (Figure 2.2b), which we surveyed biannually between 2002 and 2004 to obtain annual and seasonal variability in horizontal displacement. Displacements were calculated relative to the base station in front of bulge 1. Measurements were made in June and August of the corresponding years. Additionally, a continuously running GPS station on the bulges recorded daily positions between March and August 2003 and between June and August 2004 (GPS2003 and GPS2004 in Figure 2.2b). The continuous data were analyzed using the GIPSY/OASIS software (version GOA4) developed at the Jet Propulsion Laboratory (JPL) [*Zumberge et al.*, 1997]. We combined data from our sites with data from continuous GPS sites in and around Alaska and estimated daily positions using orbit information provided by JPL [see *Freymueller et al.*, 2000, for summary of analysis methods]. The vertical positions in ITRF2000 (International Terrestrial Reference Frame of year 2000) show vertical motions of the site relative to the geocenter, and the horizontal positions in ITRF2000 show the motion of the site relative to a nearby reference site in Whitehorse.

The horizontal displacement along profile P-P' between August 2002 and June 2003 and between August 2002 and August 2003 is shown in Figure 2.5. The mean direction of the displacements was nearly perpendicular to the glacier terminus. Over the ten-month period the sediments advanced between 15 cm near the terminus and 2 cm at the toe of the outermost bulge 1. The survey point right at the edge of the ice front was displaced 1.36 m, which is more than ten times the average. This general trend of decreasing displacements with distance from the terminus was also observed over the one-year period, although the movement of the markers across bulge 1 was irregular. Vertical motion was not detectable

within the measurement error.

Velocity calculations along the same profile showed a mean horizontal velocity of about $0.5\,\mathrm{mm\,d^{-1}}$ during summer and $0.2\,\mathrm{mm\,d^{-1}}$ during winter ('summer' refers to the time interval between the beginning of June and the end of August, 'winter' to the end of August until the beginning of June).

The continuous measurements of GPS2003 and GPS2004 gave detailed information about the displacement with time. The measurements of GPS2003 (Figure 2.6a) – close to profile P-P' – showed a clear onset of horizontal movement by the end of March. The movement was relatively steady until mid-May ($\sim 0.7\,\mathrm{mm\,d^{-1}}$), increased to $\sim 1.3\,\mathrm{mm\,d^{-1}}$ until mid June, followed by a slowdown ($\sim 0.5\,\mathrm{mm\,d^{-1}}$) and a near complete stop by the end of July. An irregular vertical motion with an amplitude of about 2 cm was detectable throughout the entire period. A similar pattern both in horizontal and vertical motion was observed at GPS2004 (Figure 2.6c). However, it was moving at higher rates than GPS2003 ($0.8\,\mathrm{mm\,d^{-1}}$ between June and August). GPS2004 was placed closer to the glacier terminus than GPS2003 and further to the east, where the glacier was very active in 2004.

During the summers of 2003 and 2004 continuous GPS receivers were also installed on the glacier surface. We calculated daily ice velocities (Appendix C). The comparison between horizontal ice velocity (Figure 2.7a) and vertical position of the sediments (Figure 2.7b) in 2004 showed an almost identical pattern until mid-July, delayed by 3-5 days. Such a correlation was not detected in 2003.

2.4.2 Internal Structure and Composition of a Bulge

We used a back-hoe to dig a trench into the toe of bulge 1, the most distal bulge that formed in 2001 (Figure 2.2b). In this 9-m-long and 6-m-deep trench we mapped the internal structure using compass and clinometer, determined the sediment composition by estimating the grain sizes in the field, and took sediment samples for which we determined the density and the water content by weighing the samples before and after being dried in an oven.

The results are summarized in Table 2.1 and Figure 2.8. The two main sedimentary facies which made up the toe of the bulge were a dry, sand-dominated upper layer including cobbles (layer 1) and clay-containing layers with higher water contents (layers 2, 4). This distinction between mud-free and mud-bearing layers could also be made in smaller trenches

and bulges eroded by water activity [*Motyka and Echelmeyer*, 2003]. The presence of water and the increasing instability of the side walls made a deeper trench impossible. Free water was observed at the interface between layer 2 (silty clay) and layer 3 (sand/silt) and water accumulated at the bottom of the trench above the compact water-rich clay layer 4.

Three types of thrust surfaces could be distinguished in the walls of the trench: (1) a nearly horizontal 5-m overthrust of sediments onto and over downslope vegetation, (2) an internal thrust with a dip angle of $\gamma = 25°$, inclined toward the glacier, and (3) an imbricate thrust system on a smaller scale (Figure 2.8). A thin film of silty clay was present along the internal thrust. Assuming that layers 2 and 4 were continuous, the horizontal offset of the internal thrust would result in a displacement of 5 m. On a smaller scale, the imbricate thrust system added a fraction of a meter (Figure 2.8b) to the shortening. The total horizontal displacement of about 5 m was within the range observed by *Motyka and Echelmeyer* [2003] in 2001. The uppermost sand-silt layer formed an anticline due to the slip along the vegetation and the internal thrust. Nevertheless, the internal layering was well-preserved.

2.5 Model of Proglacial Bulges

Between 2002 and 2004, ice-proximal deformation and small displacements across the bulges occurred simultaneously. The deformational features along the terminus as well as the strong discontinuity in the horizontal velocity across the ice margin (Figure 2.4c) were indications that the bulk strain was concentrated within a few meters of the terminus. In contrast to 2001, the force exerted by the glacier could not overcome the resistive force of the sediments in the forefield. Here we will apply the critical taper theory [*Davis et al.*, 1983; *Dahlen*, 1984] to find conditions under which either ice-proximal deformation or large scale movement prevails. With simple considerations we will propose boundary conditions which need to change for a resumption of large scale movement, as observed in 2001.

An explanation of how glaciotectonic deformation occurs must include two elements: a mechanism enabling the glacier to build up a force which is sufficiently strong to overcome the resistance of the proglacial sediments, and/or a mechanism to reduce this resistive force. We will treat this problem by making the following assumptions (Figure 2.9):

(1) A weak detachment layer exists beneath the proglacial sediments. The importance

of a weak layer within the sediments for large push moraine formation was shown e.g. by *van der Wateren* [1995]. Seismic refraction measurements in the study area and the presence of water-rich silty clay along the internal thrust within the trench (which might have been dragged along from a deeper layer during thrusting) provide evidence of a possible basal décollement.

(2) The sedimentary wedge in the push moraine area is at the critical state as defined by *Davis et al.* [1983], where a critically tapered wedge is the thinnest body that can be thrust over its basal décollement without any internal deformation. The critical taper is defined by the sum of the surface slope of the wedge (α_{sed}) and the dip of the basal décollement (β_{sed}), which we take to be $\beta_{\text{sed}} = 0$. A subcritical wedge would deform internally and thereby steepen its taper until the critical value is achieved. The geometry and mechanism of the sandbox models from which this theory was derived is similar to what we observe at Taku Glacier.

(3) The sediments are assumed to be homogeneous with a cohesionless Coulomb rheology ($|\sigma_S| = \mu_b \sigma_N$, where σ_S is the shear stress, σ_N the normal stress and μ_b the coefficient of friction at the basal décollement). The effects of anisotropy, e.g. due to clay layers within the sand, slightly increase the critical taper but have little effect on the style of deformation [*Huiqi et al.*, 1992]. Also, the cohesion can be shown to be small compared to the normal stress σ_N [*Lohrmann et al.*, 2003].

(4) The glacier profile is wedge shaped with a surface slope α_{ice} and a bed slope β_{ice}.

(5) We treat the problem two dimensionally. In the following, we use the term "force" for force per unit width.

Initiation of movement along the basal décollement happens when $F_{gl} = F_b$. We are only interested in that part of the glacier-sediment system that lies above the basal detachment layer. Therefore, F_{gl} is the horizontal glacier force acting along the glacier bed with length $\overline{BB'}$, F_b is the frictional force along the horizontal detachment layer with length L (Figure 2.9). We applied this model to two longitudinal profiles P-P" and T-T" (Figure 2.2b) extending from the glacier across the push moraines.

2.5.1 Sediment Strength

The frictional force that resists the motion of the sediments (F_b) is given by the effective normal force on the décollement (F_N) times the coefficient of basal friction μ_b, i.e.,

$$F_b = \mu_b F_N = \int_0^L \mu_b \left[\sigma_N(x) - p_f\right] \mathrm{d}x \tag{2.1}$$

where the normal stress $\sigma_N = \sigma_{zz} = \rho_{\mathrm{ice}} g h_{\mathrm{ice}}(x) + \rho_{\mathrm{sed}} g h_{\mathrm{sed}}(x)$. h_{ice} and h_{sed} are ice and sediment height, g is the gravitational acceleration and p_f the pore fluid pressure. By introducing the dimensionless quantity

$$\lambda = \frac{p_f(x)}{\sigma_N(x)} \tag{2.2}$$

we can define the pore fluid pressure as percentage of overburden pressure and rewrite equation (2.1) as

$$F_b = \mu_b F_N = \int_0^L \mu_b \left[\sigma_N(x)(1-\lambda)\right] \mathrm{d}x \,. \tag{2.3}$$

As a first approximation we take λ to equal zero. Applied to the model geometry, equation (2.1) becomes

$$F_b = \frac{1}{2}\mu_b g H_{\mathrm{sed}}^2 \left[\rho_{\mathrm{sed}} \left(\frac{1}{\tan\alpha_{\mathrm{sed}}} + \frac{1}{\tan\beta_{\mathrm{ice}}}\right) + \rho_{\mathrm{ice}} \left(\frac{\tan\alpha_{\mathrm{ice}} + \tan\beta_{\mathrm{ice}}}{\tan^2\beta_{\mathrm{ice}}}\right)\right] . \tag{2.4}$$

Note that the thickness of the glacier H_{ice} is determined by $H_{\mathrm{sed}}, \alpha_{\mathrm{ice}}$ and β_{ice}.

The inclination of the glacier surface α_{ice} and glacier bed β_{ice} are determined by linear interpolation between the elevation of the terminus and the bed and surface elevations of a location on the glacier for which radio-echo soundings of 2003 and 2004 were available, about 50 m upglacier from the margin (Appendix B). The wedge slope α_{sed} is the mean inclination between the terminus and the toe of the outermost bulge. We take $\rho_{\mathrm{ice}} = 917\,\mathrm{kg\,m^{-3}}$ and $\rho_{\mathrm{sed}} = 1800\,\mathrm{kg\,m^{-3}}$, which is the mean value of the measured densities in the trench (Table 2.1). Assumptions have to be made for the coefficient of basal friction μ_b and for the depth to the décollement layer in order to determine H_{sed}.

μ_b can be estimated with the critical taper theory. The critical taper for a dry wedge and a horizontal basal décollement $\beta_{\mathrm{sed}} = 0$ is given by

$$\alpha_{\mathrm{sed}} = \arcsin\left(\frac{\sin\phi_b}{\sin\phi_{\mathrm{int}}}\right) - \phi_b - \arcsin\left(\frac{\sin\alpha_{\mathrm{sed}}}{\sin\phi_{\mathrm{int}}}\right) \tag{2.5}$$

[*Dahlen*, 1984, equation (19) minus equation (9) therein], where ϕ_{int} and ϕ_b are the angles of internal and basal friction. Again, we use our observations within the trench to determine the coefficient of internal friction $\mu_{\text{int}} = \tan\phi_{\text{int}}$. The main thrust was dipping at an angle of $\gamma = 25°$ (Figure 2.8) and we assume the principal stress axes to be parallel and perpendicular to the sediment topography in vicinity of the surface (Figure 2.10a). The angle of internal friction $\phi_{\text{int}} = 2\theta - \frac{\pi}{2}$ is determined through the Mohr circle (Figure 2.10b), where $\theta = \frac{\pi}{2} - \alpha_{\text{sed}} - \gamma$. This results in $\phi_{\text{int}} = 32°$ or $\mu_{\text{int}} = \tan\phi_{\text{int}} = 0.6$. These values are in the general range for granular materials and were also measured by *Lohrmann et al.* [2003] in sandbox experiments. Together with $\alpha_{\text{sed}} = 4°$, the mean surface angle across the trench profile T-T", equation (2.5) leads to a coefficient of basal friction $\mu_b = \tan\phi_b = 0.2$. This is within the range of values determined by *Bowles* [1984] for soils with more than 60% clay fractions. The Taku push moraines with mean surface angles of $4 - 5°$ agree with observations in sandbox models, where glide horizons with low basal friction support wedges with narrow tapers.

A simple geometrical analysis yields the location of the décollement at 3 m HAE: In a cross-section, a rectangular area of sediments removed by shortening must equal that of the triangular pile accumulated in front of the pushing glacier. We know the present length and surface slope of the sediment wedge along profile T-T", and the distance the glacier advanced since 1996 (from the aerial photograph taken in 1996 when this area was still a flat outwash plane). Seismic refraction work in the proglacial area also delineated a strong interface at about the same depth across a broad area of our study area.

2.5.2 Horizontal Glacier Force

We separate the horizontal longitudinal glacier stress into two parts, a lithostatic stress due to overburden pressure $\rho_{\text{ice}} g h_{\text{ice}}$ and a tectonic stress due to longitudinal compression or extension σ^t_{xx}. The lithostatic stress increases proportionately with depth and the tectonic stress is assumed to be constant with depth. Therefore, the glacier force that acts on an imaginary vertical wall at the location where the basal detachment layer intersects the glacier bed (Figure 2.9), becomes

$$F_{gl} = \int_0^{H_{\text{ice}}} \left[\rho_{\text{ice}} g h_{\text{ice}}(z) + \sigma^t_{xx}\right] \mathrm{d}z = \frac{1}{2}\rho_{\text{ice}} g H^2_{\text{ice}} + \sigma^t_{xx} H_{\text{ice}} \tag{2.6}$$

We used survey markers on the ice surface, which were measured at the end of August 2003, the beginning of June 2004 and the end of August 2004, to calculate the horizontal strain rate $\dot{\epsilon}_{xx}$ in the flow direction for winter and summer. Then, we determined the tectonic stress contribution σ^t_{xx} by inverting Glen's flow law for ice [*Glen*, 1955]. For a simple estimate we equated the effective strain rate $\dot{\epsilon}_{\text{eff}}$ with $\dot{\epsilon}_{xx}$, ignoring other contributions from other stress components. The inverted Glen's flow law becomes

$$\sigma^t_{xx} = A^{-\frac{1}{n}} \dot{\epsilon}_{\text{eff}}^{\frac{1-n}{n}} \dot{\epsilon}_{xx} \approx A^{-\frac{1}{n}} \dot{\epsilon}_{xx}^{\frac{1}{n}} \tag{2.7}$$

with n=3 and the rate factor $A = 0.1\,\text{a}^{-1}\text{bar}^{-3}$ [*Truffer et al.*, 2001, and references therein].

2.5.3 Results and Sensitivity Analysis

The results of the force calculations are listed in Table 2.2. The measured geometries for both profiles result in glacier forces that are too small to overcome the resistive forces along the décollement. The glacier force is larger during winter due to a larger tectonic contribution. Critical controls that may change in order to reactivate large-scale movement along the basal décollement are (1) the glacier profile, (2) the taper of the sediment wedge and/or (3) the effective basal friction. By introducing the term 'effective basal friction' we point out that the influence of pore water in the system should not be neglected as stated in the assumptions for our model. *Hubbert and Rubey* [1959] demonstrated that the critical shear stress along a thrust plane is reduced by pore fluid pressure p_f (equation (2.1)).

The water content of the sediments (Table 2.1) shows that the sediments are not fully water saturated although water-rich layers do exist. Also, the presence of free water between layers and the abundance of water along the toes of some bulges shows that water must flow along distinct layers within the sediments. Pore fluid pressure can be enhanced either by compaction of impermeable strata (such as the clay layer observed in the trench) or transmission of water into a confined aquifer.

We computed the influence of changing boundary conditions such as $\alpha_{\text{ice}}, \beta_{\text{ice}}$, α_{sed} and λ, the ratio between pore fluid pressure p_f and overburden pressure. We changed one of these parameters while holding the others at a fixed value (equations (2.3), (2.4) and (2.6)). Because the coefficient of basal friction μ_b was estimated, we also calculated the influence of different values of μ_b on the resistive sediment force. The results are presented in Figure 2.11

for profile P-P" and Figure 2.12 for profile T-T". They show that a steepening of the glacier topography α_{ice}, a decrease in the steepness of the glacier bed β_{ice}, a steeper sediment wedge α_{sed} and the existence of water within the sediments are ways to mobilize the sediments along the basal décollement.

2.6 Discussion

The interaction of the advancing ice with its foreland took various forms: (1) the glacier overrode the proglacial area independent of the presence of a sediment pile against which the glacier could buttress (Sites B and D, Figures 2.3b,d), (2) ice and/or ice-proximal sediment ridges deformed within a few meters of the terminus (Sites A, C, E, Figures 2.3a,c and Figure 2.4) and (3) minor sediment movement occurred 200 m beyond the terminus (Figure 2.5). An explanation for these behaviors can be given with the simple model presented above. It showed that in 2004 glacier and sediment did not show a geometry favorable for major mobilization of the sediment wedge along a basal detachment layer. Here we will discuss which boundary conditions, whose modification would increase the glacier force with respect to the sediment force, are more likely to change and might be crucial for the future development of the proglacial area of Taku Glacier.

2.6.1 Model Interpretation

With the calculated $\mu_b = 0.2$ a steepening of the glacier topography α_{ice} is the most efficient way to mobilize the sediments along the basal layer (Figure 2.11a). Along profile P-P", α_{ice} needs to increase from 17° to 19°. This is more likely to happen than an increase from 11° to 20° along T-T" (Figure 2.12a). Digital elevation models which we created from aerial photographs taken in 2002 and 2003 in the terminal area show an increase of α_{ice} along P'-P" of about 2° to 3°. In addition, our observations of the deformational features along the glacier-sediment interface and the large velocity gradient across the ice-proximal ridge demonstrated that active deformation of terminal ice took place. At site D, for example, the glacier was actively steepening its surface between 2002 and 2004. It is noteworthy that an increased terminus advance does not necessarily imply surface steepening. We have observed much less ice-proximal deformation at locations with higher advance rates and a lower elevation of the terminus (site B, Figure 2.3b).

Under the assumptions of our model an increase in the steepness of the glacier bed β_{ice} results in a lower glacier to sediment force ratio (Figure 2.11b). This does not coincide with the observation that the present push moraines developed in an area where a deep trough of the glacier bed had formed upglacier from the terminus. The glacier might transmit stresses from farther upglacier than what we assumed in our model and this stress transmission might be favored by steep glacier beds. Additionally, α_{ice} and β_{ice} can not be treated as complete independent parameters. The model presented here is too simple to address this question and a flow model that couples α_{ice} and β_{ice} would be necessary.

Steepening of the sediment wedge lowers the resistive sediment force (Figure 2.11c), because of a shorter contact on the detachment layer. In our model, an increase of α_{sed} from 5° to 6° along profile P-P" is needed. With the current advance rate of the glacier terminus in the order of $10\,\mathrm{m\,a^{-1}}$ and under the assumption of a constant elevation of the terminus, the sediment wedge would achieve this taper within the next four years. This statement is not true along profile T-T" (Figure 2.12c), where an increase of α_{sed} from 4° to 16° would be necessary. However, the critical taper equation (equation (2.5)) relates an increase of the critical taper at a fixed basal friction to a decrease in internal friction. The sediment wedge might be at a subcritical state and the ongoing slow movement of the proglacial bulges might be due to internal deformation. The decreasing displacement with distance from the terminus supports this conclusion.

A pore fluid pressure of 10% of the overburden pressure at P-P" and 40% at T-T" (Figure 2.11d and 2.12d) would initiate movement. These values are reasonable for rapid water input along sediment layers with low permeability such as silty clay.

The sensitivity calculations show that reactivation of large scale deformation is more likely to happen in the area of profile P-P" (Figure 2.11) than profile T-T" (Figure 2.12). At profile P-P", a lower coefficient of basal friction μ_b than we calculated would enable slip along the basal layer under the 2004 geometry (Figure 2.11). Variability of sediment composition, changing décollement depth or variable water input within the area were not taken into account.

The critical taper theory assumes constant frictional properties. *Mulugeta and Koyi* [1992] observed episodic events in their sandbox experiments, even with constant forcing by a steadily moving backwall. They related the episodic material accretion in sandbox exper-

iments to a stick-slip mode of the décollement propagation. Figure 1 in their paper shows a similarity to the push moraine area in front of Taku Glacier despite different boundary conditions. The advancing glacier does not move steadily and its pushing front is not a rigid vertical wall. But the similarity of the observations suggests that frictional behavior might be more important than the geometry of the system. Stick-slip mode and its applicability on tectonic scales for fault reactivation during earthquakes was also described by *Marone* [1998]. *Lohrmann et al.* [2003] showed that sand exhibits a frictional behavior with strain hardening prior to failure and subsequent softening until the onset of stable movement at constant friction. We ignored such effects in our model for the Taku push moraines and might have underestimated the frictional strength. However, once the movement is initiated, a lower stable friction facilitates major events.

2.6.2 Continuous GPS Interpretation

Our results from the continuously running GPS stations on the sediments have shown an increased velocity between the end of March and the end of July (Figure 2.6a), a time that coincides with higher water input from the glacier. A spring speed up in horizontal motion beginning in April was also observed on daily ice surface velocities (Appendix D), which we relate to increased water pressure at the glacier bed. We attribute the onset of horizontal movement of the continuous sediment station GPS2003 to increasing water input into the glacier-sediment system, which was caused by an increase of the mean daily air temperature from around 0° C to 7° C during April (Figure 2.6b). The slow-down of the horizontal sediment movement by mid-June and the complete stop by the end of July as seen in 2003 and 2004 happened despite the abundance of water in the proglacial area until late August. This is quite similar to daily ice velocity observations, where the establishment of good hydraulic connections leads to lower water pressures and storage [*Paterson*, 1994]. A similar mechanism might be operating in the proglacial sediments. The correlation between horizontal glacier velocity and vertical sediment position as observed in 2004 also ceased by late July (Figure 2.7). We interpret the delay of 3-5 days between ice velocity and vertical sediment position as the reaction time the water needs to penetrate through the sediments and increase the pore fluid pressure p_f. On the other hand, we do not have a satisfactory explanation for the almost exact match of the curve shape for such a large time lag. One

would expect damping of the high frequency signals due to diffusion of water through the sediments.

Larger displacements in our cross-profile P-P' during the summer month (Figure 2.5), the fact that the 2001 movement was observed during late spring and summer [*Motyka and Echelmeyer*, 2003], and the presence of water along the internal thrust in the trench are additional arguments for the importance of water. In addition, our estimation of the tectonic contribution to the applied glacier force is larger during the winter months (Table 2.2) which extend into June. The 2003 continuous GPS data on the glacier surface (Appendix D) indicate compression into June and plug sliding afterwards. Together with an increased water pressure, the tectonic stress could have been important for the onset of sediment movement by the end of March.

2.7 Conclusions

Taku Glacier, previously a tidewater glacier, has built its terminal shoal moraine over the last 50 years. The ongoing advance has produced a series of proglacial bulges due to glaciotectonic processes. Comparison of aerial photographs and recent investigations have shown that, despite a continuous terminus advance, sediment movement is determined by few major episodic events rather than steady deformation of the glacial forefield. Several explanations for this behavior can be drawn from this study:

1. Under 2004 conditions, the applied glacier force cannot overcome the resistive force of the proglacial sediments. This is indicated by large ice deformation along the ice-sediment interface and a large velocity gradient across ice-proximal ridges. Overriding glacier ice at other locations supports this conclusion.

2. Steepening of the glacier surface is the most effective way to increase the force exerted by the glacier.

3. Enhanced sediment motion during summer, a time when water is abundant, indicates that decreased frictional resistance by infiltration of water into the system is important. Increased pore fluid pressure might play a key role in sediment movement.

4. Between 2002 and 2004 the proglacial sediments were not at the critical taper and the wedge deformed internally with the magnitude of the deformation increasing toward the terminus. The sediment wedge must shorten, and thereby increase its surface slope, to

reduce the sediment strength with respect to the force of the glacier. This could happen within as little as four years.

5. Episodic movement of the sediment wedge is related to a critical combination of several boundary conditions including inclination of the glacier surface, surface slope of the sediment wedge and pore fluid pressure within the sediments. Comparison with sandbox models shows that changing frictional conditions are a possible reason for such movements and that episodic movement is possible under steady forcing.

6. Our calculations for the glacier force involve assumptions that might be oversimplifications, because the influence of the inclination of the glacier bed does not coincide with our observations. Analyses for stress transmission within the ice and along the glacier bed may be essential. A more sophisticated model of the whole system requires a better model of the proglacial sediments.

7. Currently we do not have a good understanding of the evolution of the ice-sediment geometry, i.e. the interdependence of β_{ice} and α_{ice}. This depends on processes such as sediment excavation, which is possibly related to freeze-on and routing of subglacial water.

If the supply of ice to the terminal area of Taku Glacier continues over the next years, ice-proximal deformation might prevail until the terminal ice has reached a critical surface slope in order to increase the force of the glacier. An ongoing terminus advance in the same order as during the last two years might lower the taper of the sediment wedge and therefore reduce the resistive sediment force. On the other hand, an increased water input due to higher air temperatures or a period of heavy rainfall might be sufficient to cause the sediments to move, especially during spring when the hydraulic system within the sediments might be less established.

Acknowledgments

This study was supported by U.S. National Science Foundation, grant No. OPP-0221307. Field equipment was provided by UNAVCO and VECO Polar Resources. Free flights to the study site were sponsored by ERA helicopters. We would like to thank J.M. Amundson, E.S. Boyce, M.P. Lüthi and S. O'Neel for their help in the field, and J.T. Freymueller for his assistance with the continuous GPS analysis. K.A. Echelmeyer, W.D. Harrison and L.H. Shapiro made significant improvements to the manuscript.

Bibliography

Bennett, M. R. (2001), The morphology, structural evolution and significance of push moraines, *Earth Sience Reviews*, *53*, 197–236.

Boulton, G. S., J. J. van der Meer, D. J. Beets, J. K. Hart, and G. H. J. Ruegg (1999), The sedimentary and structural evolution of a recent push moraine complex: Holmstrombreen, Spitsbergen, *Quaternary Science Reviews*, *18*, 339–371.

Bowles, J. E. (1984), *Physical and Geotechnical Properties of Soils*, second ed., McGraw-Hill, New York.

Croot, D. G. (1987), Glacio-tectonic structures: a mesoscale model of thin-skinned thrust sheets?, *Journal of Structural Geology*, *9*(7), 797–808.

Dahlen, F. A. (1984), Noncohesive Critical Coulomb Wedges: An Exact Solution, *J. Geophys. Res.*, *89*(B12), 10,125–10,133.

Davis, D., J. Suppe, and F. A. Dahlen (1983), Mechanics of Fold-and-Thrust Belts and Accretionary Wedges, *J. Geophys. Res.*, *88*(B2), 1153–1172.

Fischer, M. P., and R. D. Powell (1998), A simple model for the influence of push-morainal banks on the calving and stability of glacial tidewater termini, *J. Glaciol.*, *44*(146), 31–41.

Freymueller, J. T., S. C. Cohen, and H. J. Fletcher (2000), Spatial variations in present-day deformation, Kenai Peninsula, Alaska, and their implications, *J. Geophys. Res.*, *105*, 8079–8101.

Glen, J. W. (1955), The creep of polycrystalline ice, *Proceedings of the Royal Society of London, Ser A*, *228*(1175), 519–538.

Hubbert, M. K., and W. M. Rubey (1959), Role of fluid pressure in mechanics of thrust faulting: I. Mechanics of fluid-filled porous solids and its application to overthrust faulting, *Geological Society of America Bulletin*, *70*, 115–166.

Huiqi, L., K. R. McClay, and D. Powell (1992), Physical models of thrust wedges, in *Thrust Tectonics*, edited by K. R. McClay, pp. 71–81, Chapman & Hall.

Humlum, O. (1985), Genesis of an imbricate push moraine, Höfdabrekkujökull, Iceland, *Journal of Geology*, *93*(2), 185–195.

Kälin, M. (1971), The active push moraine of the Thompson Glacier, Axel Heiberg Island, Canadian Arctic Archipelago, Ph.D. thesis, Swiss Federal Institute of Technology ETH Zürich, 68 p.

Krüger, J. (1985), Formation of a push moraine at the margin of Höfdabrekkujökull, south Iceland, *Geografiska Annaler*, *67 A*(3–4), 199–212.

Krüger, J. (1993), Moraine-ridge formation along a stationary ice front in Iceland, *BOREAS*, *22*, 101–109.

Lohrmann, J., N. Kukowski, J. Adam, and O. Oncken (2003), The impact of analogue material properties on the geometry, kinematics, and dynamics of convergent sand wedges, *Journal of Structural Geology*, *25*, 1691–1711.

Marone, C. J. (1998), Laboratory-derived friction laws and their application to seismic faulting, *Annual Review Earth Planet Science*, *26*, 643–696.

Meier, M. F., and A. Post (1987), Fast tidewater glaciers, *J. Geophys. Res.*, *92*(B9), 9051–9058.

Motyka, R., E. Kuriger, and M. Truffer (2005), Excavation of sediments by tidewater glacier advance and implications fo the oceanic sediment record, Taku Glacier, Alaska, USA, *Geophysical Research Abstracts, EGU Spring Meeting 2005*, abstract.

Motyka, R. J., and J. E. Begét (1996), Taku Glacier, southeast Alaska, U.S.A.: Late Holocene history of a tidewater glacier, *Arctic and Alpine Research*, *28*(1), 42–51.

Motyka, R. J., and K. A. Echelmeyer (2003), Taku Glacier (Alaska, U.S.A.) on the move again: active deformation of proglacial sediments, *J. Glaciol.*, *49*(164).

Mulugeta, G., and H. Koyi (1992), Episodic accretion and strain partitioning in a model sand wedge, *Tectonophysics*, *202*(2–4), 319–333.

NASA (1979), U2-flight, archived at: GeoData Center, Geophysical Institute, University of Alaska Fairbanks, unpublished. Frame Number 4259–4260.

Nolan, M., R. J. Motyka, K. A. Echelmeyer, and D. C. Trabant (1995), Ice thickness measurements of Taku Glacier, Alaska, USA, *J. Glaciol.*, *41*(139).

Paterson, W. S. B. (1994), *The Physics of Glaciers*, third ed., 481 pp., Butterworth-Heinemann, Oxford.

Post, A., and R. J. Motyka (1995), Taku and LeConte Glaciers, Alaska: calving speed control of Late-Holocene asynchronous advances and retreats, in *William O. Field Festschrift*, pp. 59–82, Physical Geography, University of Alaska Fairbanks.

Sharp, M. (1984), Annual moraine ridges at Skálafellsjökull, South-east Iceland, *J. Glaciol.*, *30*(104), 82–93.

Truffer, M., K. A. Echelmeyer, and W. D. Harrison (2001), Implications of till deformation on glacier dynamics, *J. Glaciol.*, *47*(156), 123–134.

U. S. National Ocean Service (1989), archived at: GeoData Center, Geophysical Institute, University of Alaska Fairbanks, unpublished. Frame Number A6-175, A6-176.

U.S.D.A. Forest Service (1996), photo acquired by NASA, archived at: Forest Service Information Center, Juneau, unpublished.

van der Wateren, D. F. M. (1995), Structural geology and sedimentology of push moraines: processes of soft sediment deformation in a glacial environment and the distribution of glaciotectonic styles, *Mededelingen Rijks Geologische*, *54*.

Zumberge, J. F., M. B. Heflin, D. C. Jefferson, M. M. Watkins, and F. H. Webb (1997), Precise point positioning for the efficient and robust analysis of GPS data from large networks, *J. Geophys. Res.*, *102*, 5005–5018.

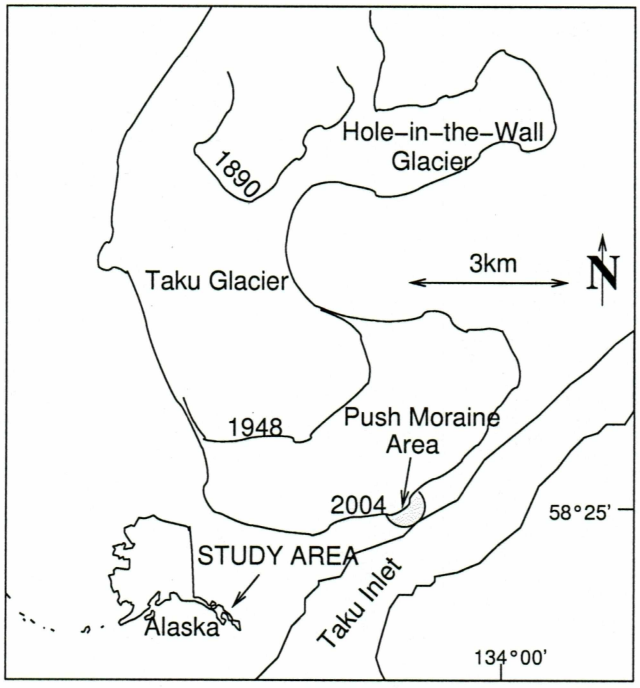

Figure 2.1. Terminus area of Taku Glacier. The glacier started to readvance in 1890. Until 1948, the glacier was calving into the fjord along its entire terminus. Since then, the area of ice-proximal moraines and uplifted sediments increased continuously and a major push moraine complex developed above sea level at the central part of the terminus.

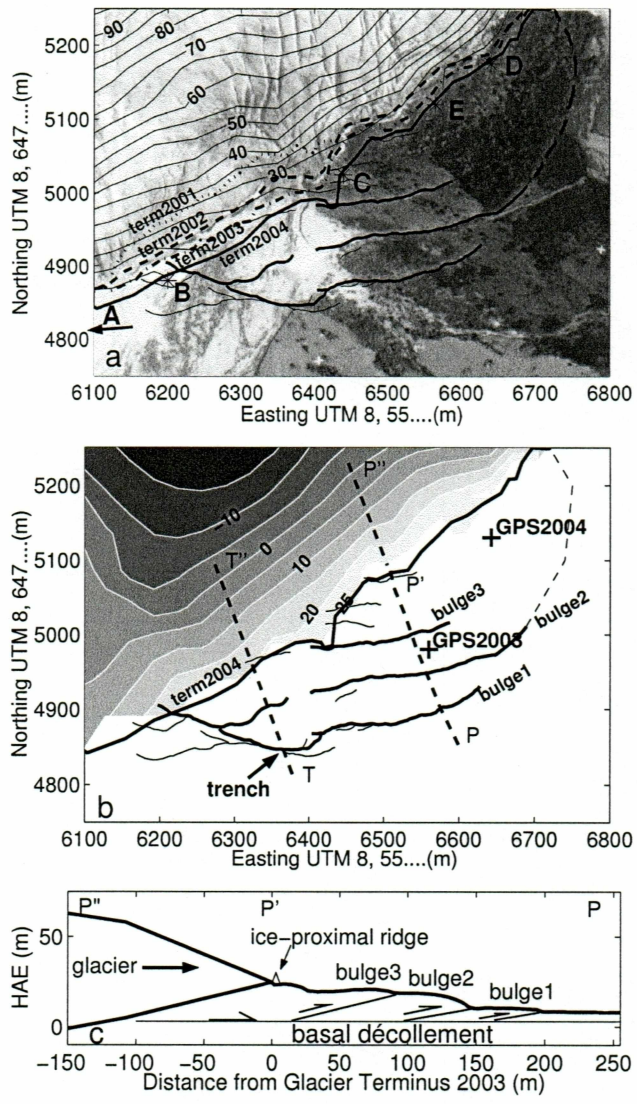

Figure 2.2. Push moraine area in front of Taku Glacier. (a) Orthophoto 2002 with terminus positions from 2001 to 2004. The contour lines represent the topography of the glacier surface near the terminus (m HAE). The toes of the bulges are shown with solid lines where measured and a dashed line where inferred. Points A–E refer to sites where different deformational features at the glacier-sediment interface were observed (note that A is 400 m west of figure boundary). (b) Map view with the contour lines of the glacier bed (m HAE). GPS2003 and GPS2004 are the locations of continuously running GPS. "trench" shows the location where a trench was dug, and T-T" and P-P'-P" show profiles discussed in the text. (c) Cross profile along profile P-P".

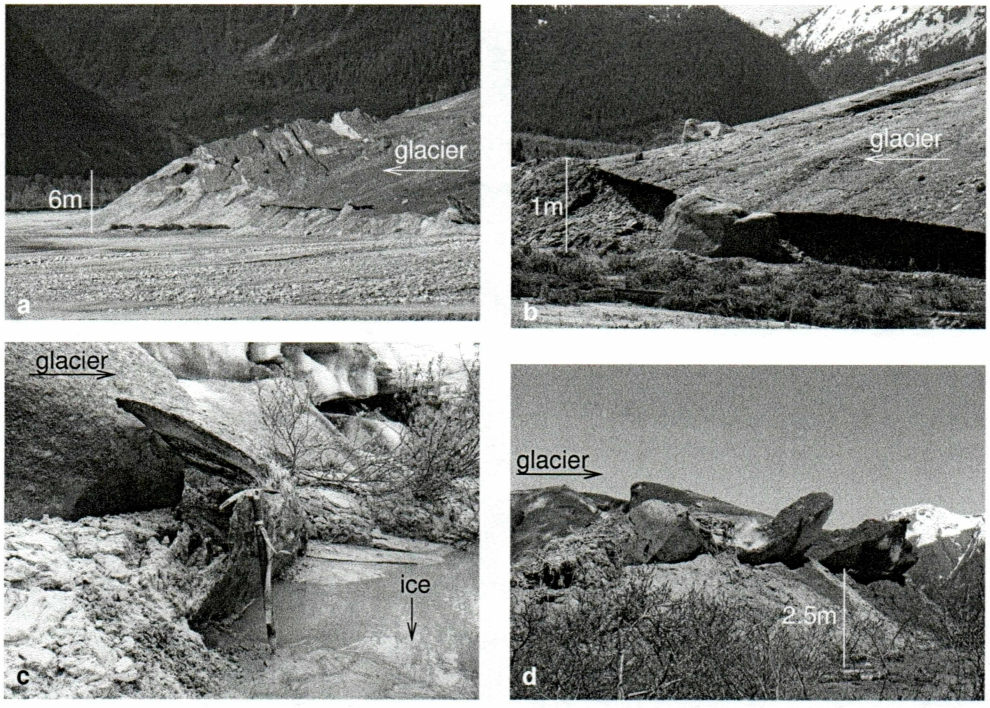

Figure 2.3. Deformation at the glacier-sediment interface. (a) Site A, 30 August 2004: A 6-m-high sediment ridge causes the advancing ice to form upglacier dipping imbricate thrusts. (b) Site B, 29 May 2004: The glacier overrides the foreland and a 1-m-high sediment ridge. (c) Site C, 11 June 2004: A sliver of ice about 10-cm-thick is detached from the subjacent ice (under the water) and folded back toward the glacier. (d) Site D, 15 May 2004: The advancing ice overrides a 2.5-m-high ice-proximal ridge.

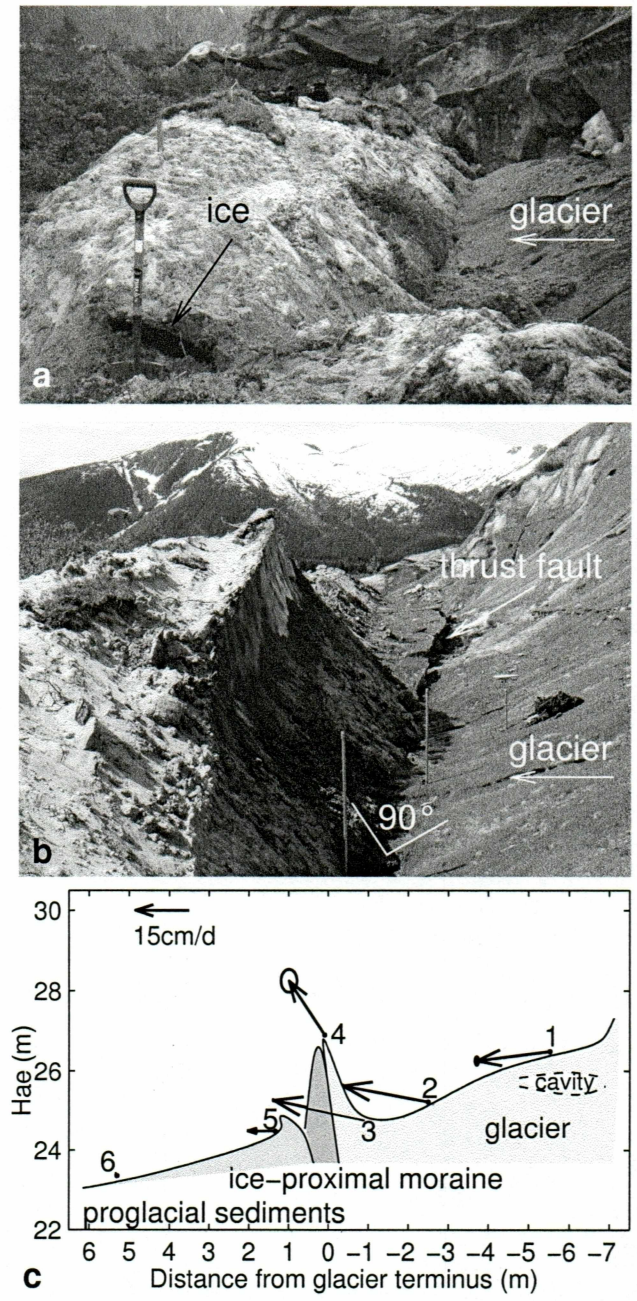

Figure 2.4. Deformation at the glacier-sediment interface Site E. (a) 15 June 2003: a 3-cm-thick sliver of advancing ice undercuts vegetation and sediments. (This picture is reversed for clarity.) (b) The same site 8 June 2004: ice-cored sediment ridge with the ice forming a slab, tens of cm thick, that moves almost vertically upward. It is connected to the glacier at an angle of roughly 90°. Several meters to the side, the terminal ice forms thrust faults. (c) velocity cross-profile June 2004: arrows indicate direction and speed at different locations with the corresponding error-ellipses. The vertical velocity of $13.5\,\mathrm{cm\,d^{-1}}$ of the ice slab (point 4) equals the ablation rate at this location. A 60-cm-thick cavity was detected below survey marker 1.

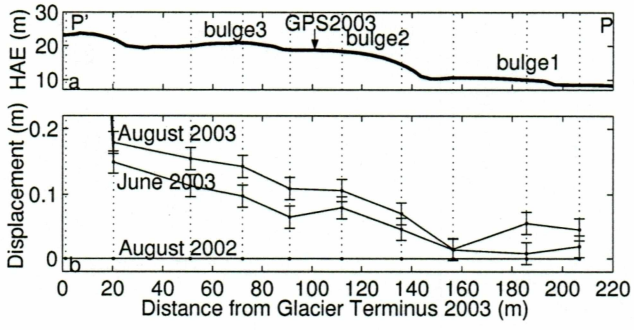

Figure 2.5. Horizontal displacement along cross-profile P-P' (Figure 2.2). (a) The topography along the profile is vertically exaggerated. The approximate location of the continuous GPS2003 is indicated by arrow. (b) Horizontal displacement was calculated with respect to August 2002. The middle line shows the displacement after ten months, the upper line after one year. The error range is displayed by vertical lines. The measurement of a survey point 2 m away from the terminus is not plotted, since it was an order of magnitude larger than the others.

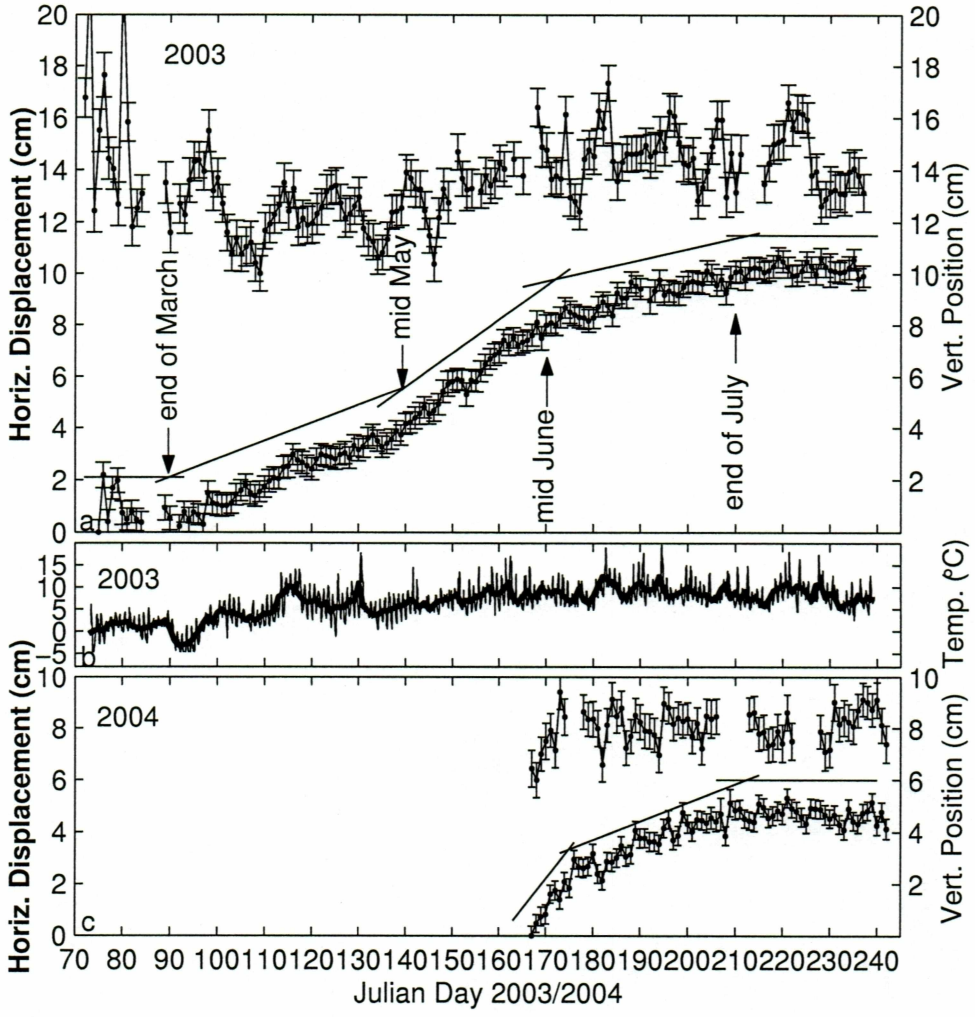

Figure 2.6. Continuous GPS measurements on the bulges 2003/2004. (a) Daily position measurements on the proglacial bulges at location "GPS2003" and (c) at location "GPS2004". The upper lines in each figure show the vertical position with respect to an arbitrary point of origin, the lower lines the horizontal displacement with respect to the first measurement. The corresponding errors are indicated with vertical lines. (b) Air temperature measured close to GPS2003.

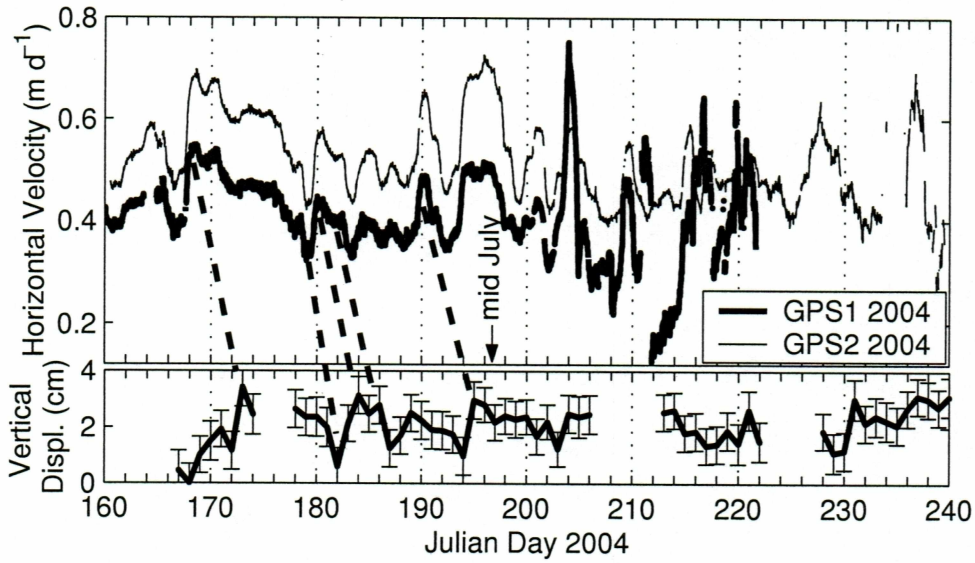

Figure 2.7. Comparison of daily sediment and ice movement 2004. (a) Daily horizontal velocity at two locations on the glacier surface. "GPS1 2004" was located about 500 m, "GPS2 2004" about 700 m upglacier from the terminus. After Julian Day 210 the data became noisier due to surface ablation and therefore increasingly unstable GPS antennas. (b) Daily vertical position with error bars at location "GPS2004" on the proglacial sediments, with respect to an arbitrary point of origin.

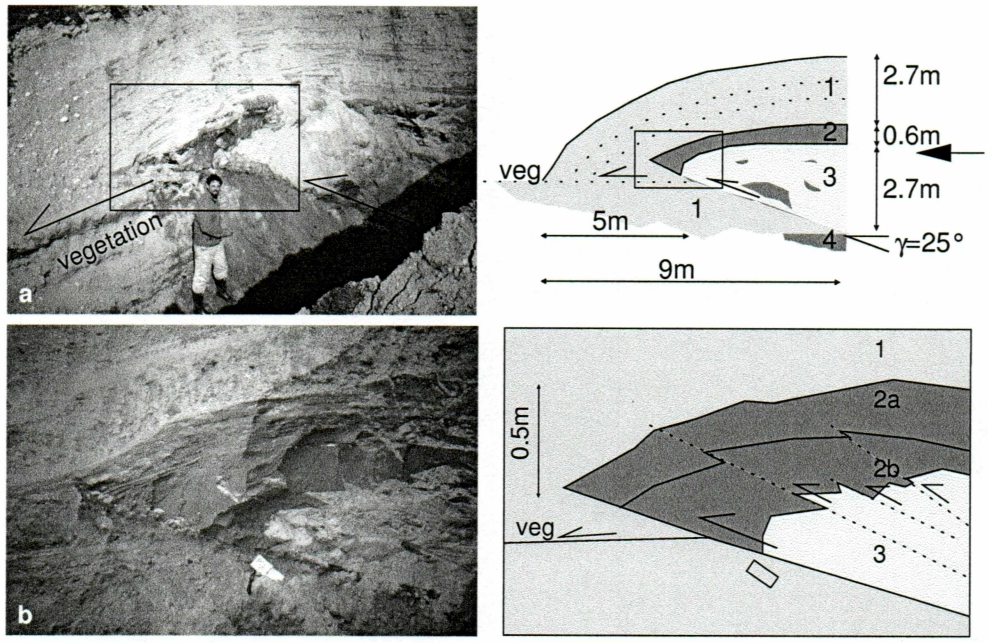

Figure 2.8. Trench at the toe of bulge 1. The 9-m-long and 6-m-deep trench revealed four sediment layers: sand-silt with cobbles with a low water content (1), laminated silty clay and compact clay with high water contents (2a, 2b), sand-silt with clay lenses (3), compact silty clay rich in water (4). See Table 2.1 for details. (a) The primary structural features were a horizontal thrust over the undeformed vegetation and an internal upglacier dipping thrust. The rectangular box is enlarged in (b) and shows a fan of imbricate thrusts on a smaller scale. Images taken on 27 August 2003.

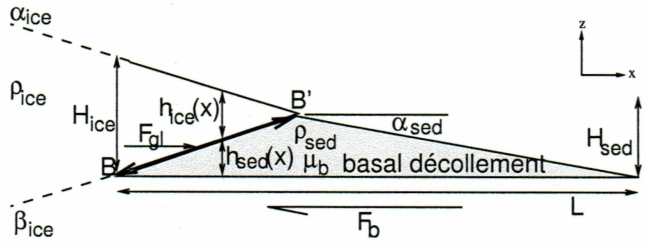

Figure 2.9. Idealized model of glacier and sediment geometry in the push moraine area used for profiles P-P" and T-T". Initiation of movement along the basal décollement happens as soon as $F_{gl} = F_b$. The horizontal glacier force acts along the glacier bed with length $\overline{BB'}$. H_{sed} defines the maximum height of the sediment pile, H_{ice} the maximum glacier height, both above the décollement.

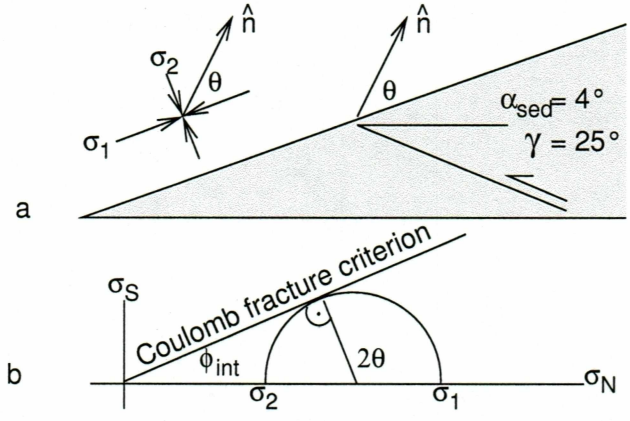

Figure 2.10. Determination of the angle of internal friction ϕ_{int}. (a) Sketch of the sediment wedge, showing the directions of principle stresses σ_1, σ_2, the unit normal $\hat{n}$ to the thrust fault, the dip angle γ of the thrust fault within the trench and the mean surface angle α_{sed} across profile T-T". (b) Mohr circle to calculate the angle of internal friction ϕ_{int}.

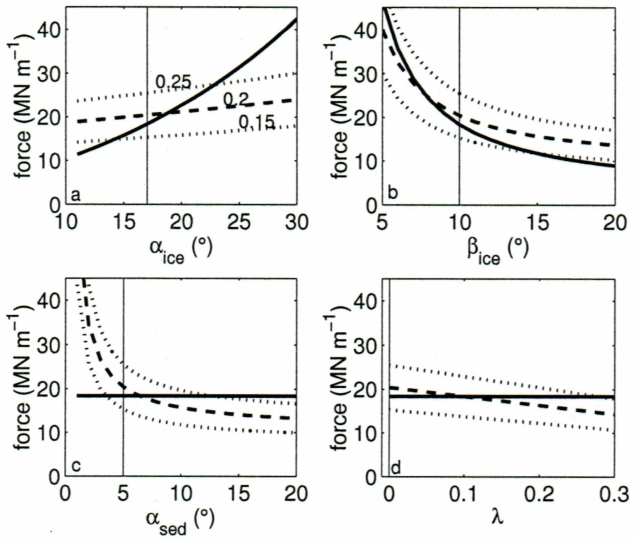

Figure 2.11. Sensitivity analysis profile P-P". Sensitivity of the resistive sediment force (dashed lines) and applied glacier force (solid lines) with respect to the parameters α_{ice} (a), β_{ice} (b), α_{sed} (c) and λ (d) along profile P-P". The vertical lines mark the parameter values found for the 2004 geometry or, in (d), the assumptions made in our model. Dotted lines show the sediment force calculated with a higher or lower coefficient of basal friction μ_b than the one resulting from the critical taper theory. Points where the solid and dashed/dotted lines intersect provide values of the corresponding parameter necessary to initiate basal movement.

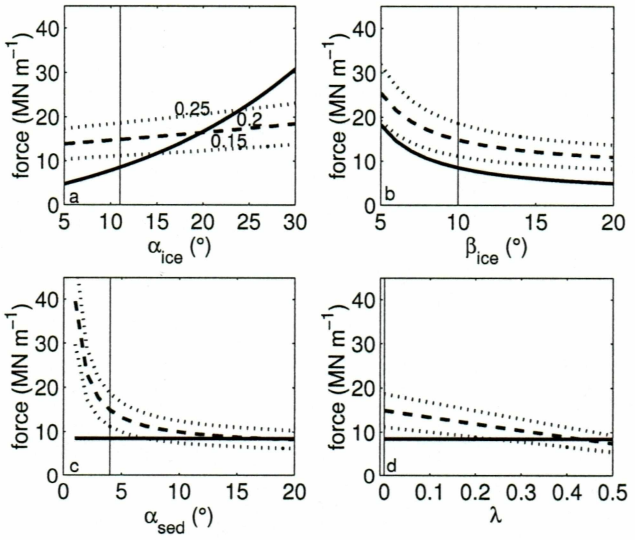

Figure 2.12. Sensitivity analysis profile T-T", same as Figure 2.11.

Table 2.1. Sediment types within the trench. Numbers in column 1 correspond to Figure 2.8.

	Sediment composition	thickness (m)	density (kgm^{-3})	water content (by weight)	special characteristics
top					
1	sand/silt with cobbles	2.7	1650	4 %	cross-bedding
2a	silty clay	0.2	1850	35 %	laminated
2b	clay	$0.2 - 0.5$		26 %	compact
3	sand/silt with clay lenses	2.5	1820	19 %	
4	silty clay	?	2005	30 %	compact, water rich
bottom					

Table 2.2. Resistive sediment force F_b versus applied glacier force F_{gl} for cross-profiles T-T" and P-P" (Figure 2.2).

		profile T-T"	profile P-P"
sediments	F_b	$14.9\,\mathrm{MN\,m^{-1}}$	$20.4\,\mathrm{MN\,m^{-1}}$
	α_{sed}	4°	5°
	H_{sed}	18 m	21.5 m
	μ_b	0.2	0.2
glacier	F_{gl} (summer)	$8.44\,\mathrm{MN\,m^{-1}}$	$18.3\,\mathrm{MN\,m^{-1}}$
	F_{gl} (winter)	$9.44\,\mathrm{MN\,m^{-1}}$	$19.3\,\mathrm{MN\,m^{-1}}$
	F_{lith}	$6.44\,\mathrm{MN\,m^{-1}}$	$15.5\,\mathrm{MN\,m^{-1}}$
	F_{tect} (summer)	$2.0\,\mathrm{MN\,m^{-1}}$	$2.8\,\mathrm{MN\,m^{-1}}$
	F_{tect} (winter)	$3.0\,\mathrm{MN\,m^{-1}}$	$3.8\,\mathrm{MN\,m^{-1}}$
	α_{ice}	11°	17°
	β_{ice}	10°	10°

Chapter 3
General Conclusion

Taku Glacier, previously a tidewater glacier, has built its terminal shoal moraine over the last 50 years. The ongoing advance has produced a series of proglacial bulges due to glaciotectonic processes. Comparison of aerial photographs and recent investigations have shown that, despite a continuous terminus advance, sediment movement is determined by few major episodic events rather than steady deformation of the glacial forefield. Several explanations for this behavior can be drawn from this study:

1. Under 2004 conditions, the applied glacier force cannot overcome the resistive force of the proglacial sediments.

2. Steepening of the glacier surface is the most effective way to increase the force exerted by the glacier.

3. Enhanced sediment motion during summer, a time when water is abundant, indicates that decreased frictional resistance by infiltration of water into the system is important.

4. The sediment wedge must shorten, and thereby increase its surface slope, to reduce the sediment strength with respect to the force of the glacier.

5. Episodic movement of the sediment wedge is related to a critical combination of several boundary conditions including inclination of the glacier surface, surface slope of the sediment wedge and pore fluid pressure within the sediments.

Taku Glacier has provided a unique opportunity to study glaciotectonic processes within a timescale suitable for scientific research. This is in contrast to investigations on tectonic scales like accretionary wedges and fold-and-thrust belts, which show a similar geometry. The advantage of having a "natural lab", like Taku Glacier, is that different methods can be applied to investigate ongoing processes. In this study, mainly three different methods were used to study the episodic movement of the Taku push moraines. The first was of descriptive nature, where the various deformational features of ice and sediments along the terminus were described. Secondly, GPS measurements across the terminus and in the proglacial area provided quantitative results. Together with a simple model, the combination of observations and measurements lead to a possible interpretation for the episodic nature of the sediment movement.

Additional measurements which were only partly included in chapter 2 and described briefly in the appendices A to G might contribute significantly to further investigations and give a better insight into the behavior of the Taku push moraines. Additional methods, which have not been applied yet, might provide information about processes such as water infiltration into the sediments. According to this study, the influence of water is important for the evolution of the push moraines. The installation of pressure transducers in ice and sediments, together with simultaneous velocity measurements, would provide the most necessary information for a better understanding of the observations presented in this study.

Appendix A

Picture Gallery

Figure A.1. Picture gallery I, trench. 26-28 August 2004. The numbers refer to Table 2.1. (a) Glacier moves from right to left, the arrow points to the vegetated surface over which the bulge thrust in 2001. (b)–(f) Details within the trench. The bright layers contain mainly sand and silt, the water rich clay/silt layers are of darker color. The arrow in (f) points to possible water escape structures during loading and compaction.

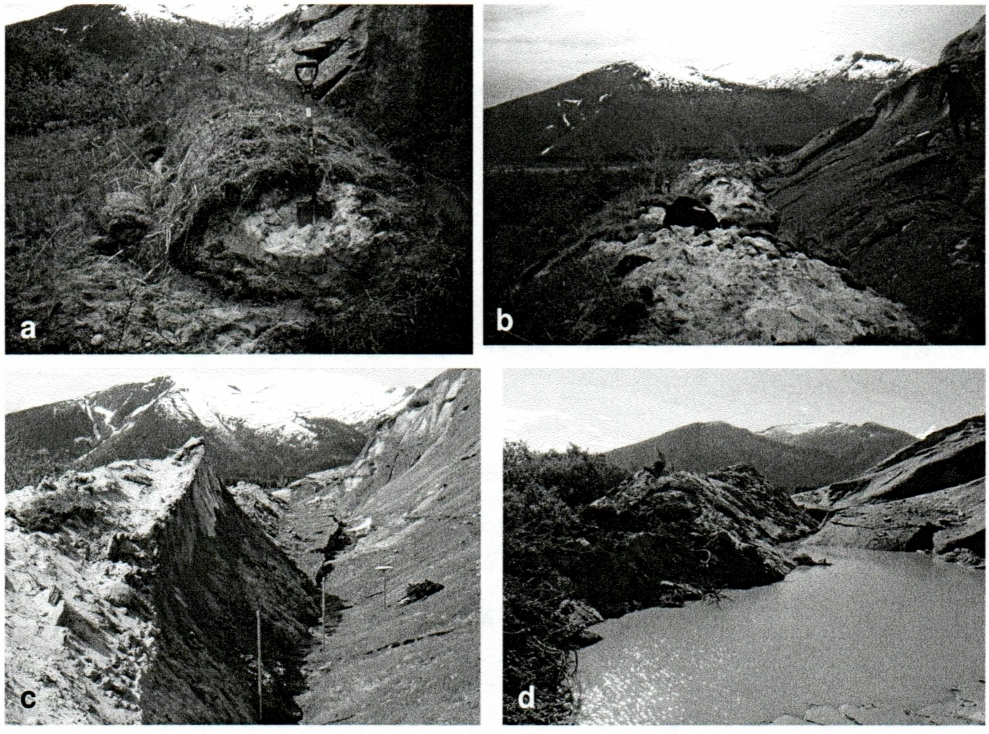

Figure A.2. Picture Gallery II, time sequence Site E. See also Figures 2.2 and 2.4. (a) and (b): 15 June 2003: Vegetation becomes folded and lifted by the advancing ice. (c) 8 June 2004: A slab of ice moves almost vertically upward. (d) 30 August 2004: The ice retreated back by the end of the summer, though slabs of ice are still detectable within the sediment ridges.

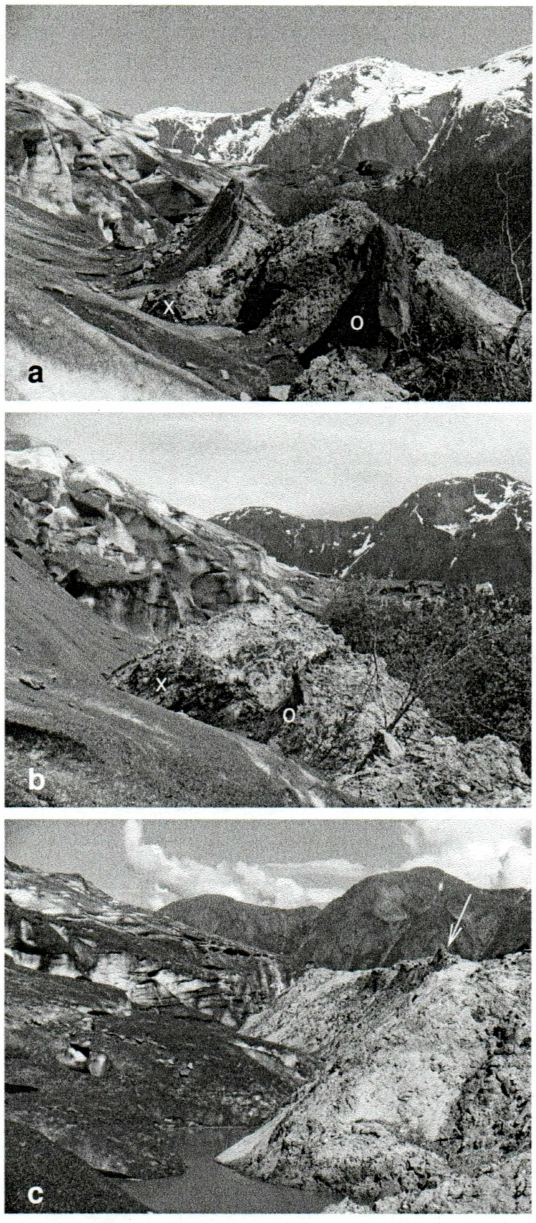

Figure A.3. Picture Gallery III, time sequence west of Site E. (a) 15 May 2004: Slivers of ice move vertically upward along the ice proximal part of the ridge. (b) 13 June 2004: Unlike at nearby Site E, the ablation of the ice slabs is higher than the vertical motion and they start retreating by June. "x" and "o" mark the same location in (a) and (b). (c) 30 August 2004: The glacier retreated back, but ice slabs are still moving within the sediment ridge (arrow). Their ablation is presumably inhibited by the sediment cover.

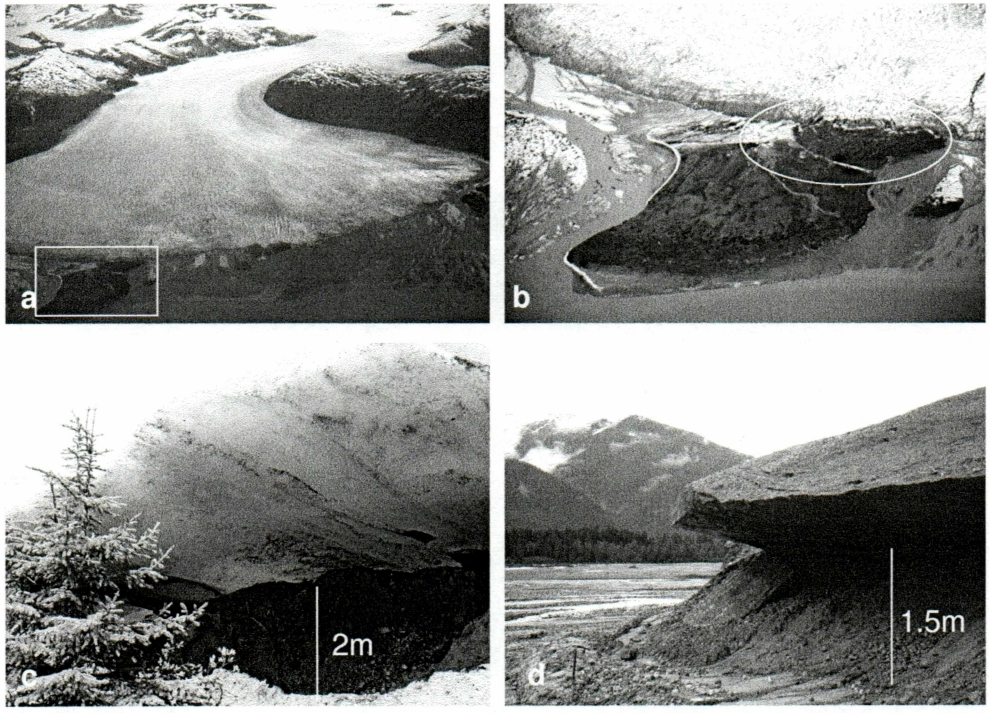

Figure A.4. Picture Gallery IV. (a) 7 June 2004: Terminal area of Taku Glacier. The study site is in the lower left corner of the picture (rectangle) and enlarged in (b) 7 June 2004: Study site with the area of the push moraines (ellipse). (c) 8 June 2004: Advancing Taku Glacier, terminus near profile P-P'. (d) 23 August 2003: Part of the advancing ice broke away and is about to be overridden by the ongoing advance, $\sim$ 20 m west of Site B (Figure 2.2).

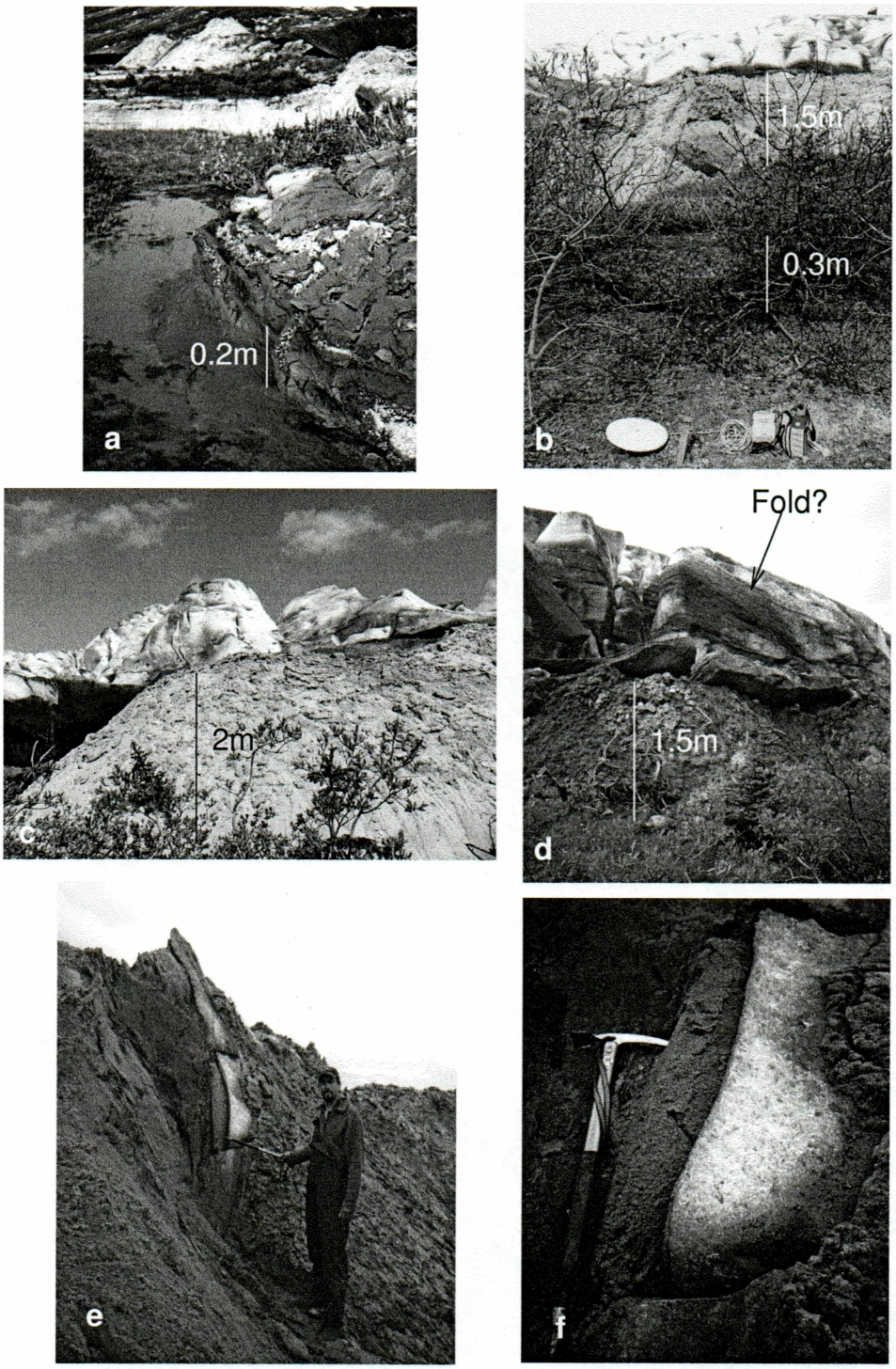

Figure A.5. Picture Gallery V. (a) 12 June 2003: Vegetation at the very terminus becomes folded. Glacier flows from right to left. (b) 22 May 2004: Near Site D (Figure 2.2) where the glacier overrides a sediment ridge, in front of which vegetation becomes folded. The glacier moves toward the camera. (c) 8 June 2004: terminus near profile P-P'. (d) 15 June 2004: Folded dirty ice within the terminal ice?, near Site D (Figure 2.2). (e) 24 August 2003: Sliver of ice along the ice proximal part of a sediment ridge at the very terminus, $\sim 300\,\mathrm{m}$ east of the push moraine area, enlarged in (f) 24 August 2003: A silt layer is squeezed out by the ice slab.

Figure A.6. Picture Gallery VI. (a) 16 June 2003: The only calving section along the terminus of Taku Glacier, where the Norris River erodes the ice. (b) 23 August 2003: Site A (Figures 2.2 and 2.3a), looking eastward. (c) 27 May 2004: Looking westward from the push moraine area toward Site A. (d) August 2004: Glacier bed, where water runs between a thin dark bubbly-free ice layer and bubbly glacier ice. (e) 12 June 2003: slab of ice at Site D. (f) 12 June 2003: Site D, depression that will be completely ice filled by June 2004 (Figure 2.3d).

Appendix B
Radio-Echo Sounding

During summer 2003 and 2004 radio-echo soundings were made with a ~ 5 MHz mono-pulse system in the terminal area of Taku Glacier. The antennas were oriented perpendicular to the ice flow with a spacing of about 30 m. Using an electromagnetic wave velocity of $168\,\mathrm{m}\mu\mathrm{s}^{-1}$ (clean ice) the reflector depth could be determined from the travel time of the first return of the electromagnetic wave.

The glacier bed topography in the terminal area of Taku Glacier is shown in Figure B.1 and revealed a 120 m deep trough upglacier from the push moraine area.

All soundings are summarized in Table B.1. These data and additional information are included in the data CD (Appendix G and CD in back pocket).

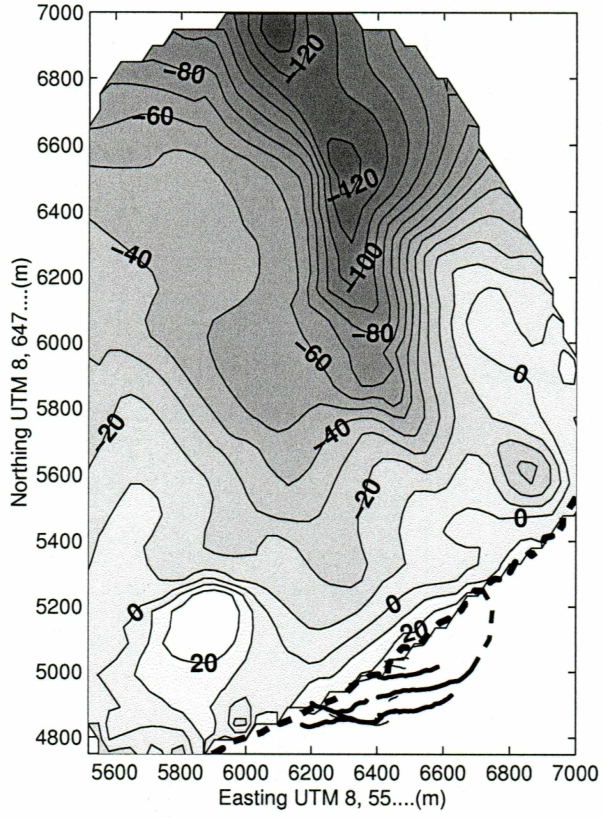

Figure B.1. Contourlines of glacier bed topography. The bed elevation of the terminal area of Taku Glacier is in height above ellipsoid (HAE).

Table B.1: Radio-echo soundings in the terminal area of Taku Glacier, 2003 and 2004: positions, distance between transmitter and receiver (Δ d), return times (Δ t) and calculated bed elevation (NaN where unreasonable value). In 2003, the positions were measured with a handheld GPS (vertical accuracy less than 10m), the surface elevation corrected with a digital elevation model (DEM) created form aerial photographs 2003 (except No. 1-13, 26, 44, 53. 55. 60, 64). The 2004 positions were measured with precision GPS.

No.	Northing (m)	Easting (m)	Surface HAE (m)	Δ d (m)	Δ t (μs)	Bed HAE (m)
2003						
1	6479165	552472	350	34.5	3.68	NaN
2	6479194	552616	350	32	5.7	−137
3	6479305	552849	350	27	2.76	NaN
4	6479322	552947	350	32	5.96	−159
5	6479361	553105	350	30	2.16	NaN
6	6479379	553312	350	30	7.2	−263
7	6479442	553485	350	30	7.16	−260
8	6479494	553779	350	32.5	3.08	NaN
9	6479537	554002	350	31.5	3.88	−163
10	6479613	554284	350	30.5	2.4	−92
11	6478368	555074	271	32	5.04	−161
12	6478435	555279	260	30	5.5	−210
13	6478506	555506	249	34	4.6	−147
14	6476980	556090	203	28	4	−141
15	6477045	556199	197	30	3.6	−114
16	6476946	555910	205	33	3.48	−96
17	6476256	556240	151	30	2.76	−89
18	6476003	556368	139	27	2.48	−76
19	6475912	556412	134	30	2.44	−79
20	6475831	556460	130	30	2.24	−66
21	6475764	556485	130	34	2	−49
22	6475989	556489	138	25	1.92	−30
23	6475948	556287	136	30	2.32	−67
24	6475890	556215	133	31	2.16	−57
25	6475836	556132	131	31.5	2.12	−55
26	6475794	556055	138	37.5	2.04	−43
27	6475726	555963	133	27	2	−42
28	6475652	555887	134	30	1.8	−25
29	6475578	555962	121	29.5	1.68	−28
30	6475494	556020	112	26.5	1.6	−30
31	6475395	556068	109	27	1.32	−8
32	6475265	556057	95	26	1.2	−12

Table B.1: Continued

No.	Northing (m)	Easting (m)	Surface HAE (m)	Δ d (m)	Δ t (μs)	Bed HAE (m)
33	6475150	556065	77	32	0.8	3
34	6474868	555701	54	31	0.52	4
35	6474812	555719	42	23	0.48	−3
36	6474988	555653	77	31	0.72	10
37	6475069	555628	87	34	0.96	−1
38	6475156	555592	95	31	1.08	−3
39	6475263	555554	104	23.5	1.2	−3
40	6475386	555567	114	31.5	1.36	−8
41	6475465	555668	120	29	1.44	−8
42	6475524	555756	124	30	1.52	−11
43	6475553	555827	125	30	1.56	−14
44	6475405	555792	115	28.5	1.44	−13
45	6475319	555847	103	34.3	1.32	−16
46	6475228	555903	98	34	0.72	30
47	6474950	556011	50	27	0.48	4
48	6474916	555911	48	26.2	0.4	10
49	6474869	555816	47	32	0.36	11
50	6474952	556108	39	30	0.36	4
51	6475020	556078	54	35	0.56	0
52	6475038	556164	48	30	0.48	1
53	6475052	556257	45	36	0.32	13
54	6475114	556226	55	30	0.68	−8
55	6475232	556173	72	31	1	−19
56	6475349	556114	101	23	1.32	−16
57	6475427	556137	111	30	1.5	−23
58	6475296	556452	71	30	0.88	−10
59	6475367	556501	69	30	0.84	−9
60	6475258	556593	49	30	0.44	6
61	6475186	556466	58	27	0.56	5
62	6475394	556386	85	30.5	1.12	−17
63	6475461	556373	98	31	1.28	−17
64	6475555	556365	118	30	1.56	−21
65	6475651	556339	123	30	1.7	−27
66	6475750	556333	126	28	1.84	−36
67	6475869	556319	130	30	1.92	−39
68	6475756	557042	40	30	0.44	−3
69	6475841	556973	66	30	0.6	9
70	6475893	556886	86	30	0.92	1
71	6475961	556794	106	26	1.16	2
72	6476067	556740	118	26	1.28	4
73	6476162	556722	125	30	1.4	0

Table B.1: Continued

No.	Northing (m)	Easting (m)	Surface HAE (m)	Δd (m)	Δt (μs)	Bed HAE (m)
74	6476056	556674	128	30	1.42	1
75	6476190	556849	121	33	1.44	−8
76	6476926	556106	194	30.5	3.84	−136
77	6476926	556106	194	30.5	3.96	−147
78	6476840	556072	197	27	3.48	−103
79	6476690	556115	178	32.5	3.2	−99
80	6476690	556115	178	32.5	3.32	−109
81	6476496	556172	168	28	2.76	−72
82	6476496	556172	168	28	2.92	−85
83	6476355	556165	154	30	2.5	−64
84	6476225	556175	149	30	2.44	−64
85	6476154	556146	152	30	2.4	−58
86	6476064	556186	144	30	2.36	−62
87	6475890	556170	135	30	1.9	−33
88	6475890	556170	135	30	2.04	−45
89	6475900	556196	134	30	2.08	−48
90	6475913	556220	135	30	2.04	−44
91	6475708	556220	124	30	2.04	−55
92	6475511	556237	114	25	1.68	−34
93	6475383	556280	95	25	1.36	−26
94	6475276	556359	75	20	1.08	−21
2004						
1	6475600.998	556876.777	50.57	31	0.9	−32
2	6475752.39	556907.691	74.66	33	0.8	0
3	6475793.671	556688.959	109.53	31	1.36	−12
4	6476075.976	556559.369	148.56	33	2	−28
5	6476250.974	556563.297	155.19	25	2.04	−23
6	6476303.594	556661.007	141.67	34	1.84	−22
7	6476529.365	556756.487	162.52	33	2.38	−46
8	6476732.665	556663.715	181.01	23	2.96	−74
9	6476922.381	556516.825	188.78	32	3.12	−82
10	6476422.377	556836.096	142.71	27	2.12	−42
11	6476241.831	556812.184	134.66	33	1.72	−18
12	6476075.181	556890.542	116.75	38	1.32	−3
13	6475959.698	556987.27	97.54	30	0.95	11
14	6475845.987	557057.466	59.17	27	0.62	1
15	6475482.08	556758.888	54.78	30	0.58	−1
16	6475364.036	556738.666	36.22	27	0.36	1
17	6476209.765	555996.954	168.22	30	2.48	−48
18	6476325.202	555922.801	178.26	27	2.6	−47
19	6476463.885	555854.445	192.04	29	2.76	−47

Table B.1: Continued

No.	Northing (m)	Easting (m)	Surface HAE (m)	Δ d (m)	Δ t (μs)	Bed HAE (m)
20	6476558.538	555862.633	190.43	32	2.76	−50
21	6475860.078	555665.208	166.03	30	2.14	−22
22	6476053.76	555548.366	179.07	38	2.42	−34
23	6476419.056	555486.639	201.08	24	2.8	−41
24	6476641.258	555513.705	216.93	43	3.16	−60
25	6476824	555568	206	29	3.24	−74
26	6476978.958	555815.293	207.03	33	3.48	−94
27	6476858.009	556029.287	196.73	35	3.6	−115
28	6476741.924	556165.059	194.82	30	3.6	−116
29	6476465.859	556307.046	179.05	32	3.48	−122
30	6476078.092	556430.224	153.54	31	2.72	−83
31	6476206.55	556327.14	160.86	33	3.04	−103
32	6476115.864	556166.162	158.05	33	2.56	−66
33	6476019.318	555806.601	165.31	41	2.4	−47
34	6475412.093	556037.92	117.34	28	1.6	−24
35	6475509.188	556131.762	123.03	36	1.8	−37
36	6475585.002	556298.752	126.86	30	1.75	−28
37	6475685.737	556405.927	132.06	30	1.76	−23
38	6475522.809	556418.566	114.1	29	1.6	−28
39	6475476.855	556398.646	107.01	30	1.42	−20
40	6475398.793	556258.485	106.1	30	1.48	−26
41	6475055.445	556180.352	54.48	34	0.63	−6
42	6475205.014	556289.102	70.4	30	0.94	−16
43	6475307.691	556339.675	88.02	31	1.24	−24
44	6475288.479	556421.737	80.99	33	1	−11
45	6475391.354	556483.722	82.5	32	0.9	−1
46	6475447.599	556642.671	67.48	28	0.7	2
47	6475299.704	556654.176	37.13	34	0.4	−2
48	6475075.564	556418.865	44.12	34	0.28	16
49	6475793.871	556037.604	141.48	36	2.2	−53
50	6475902.951	556190.159	142.34	35	2.12	−45
51	6475928.863	556517.411	141.17	35	2.06	−41
52	6475895.092	556421.108	138.9	40	2.4	−73
53	6475840.886	556338.463	135.7	32	2.28	−64
54	6475785.548	556234.248	133.92	37	2.04	−47
55	6475701.778	556011.673	136.85	35	2	−40
56	6475621.176	556137.082	125.82	28	1.92	−43
57	6475618.249	556309.601	128.78	33	1.92	−41
58	6475783.167	556392.523	134.42	27	2.04	−44
59	6475008.987	555496.373	89.47	26	1	−1
60	6474918.268	555549.322	76.03	30	0.88	−5

Table B.1: Continued

No.	Northing (m)	Easting (m)	Surface HAE (m)	Δ d (m)	Δ t (μs)	Bed HAE (m)
61	6474815.393	555587.275	56.5	25	0.56	4
62	6474687.39	555543.186	28.63	26	0.48	−17
63	6474717.727	555640.408	23.82	34	0.42	−18
64	6474745.848	555801.673	18.27	28	0.34	−15
65	6474823	555986.253	19.79	31	0.36	−16

Appendix C
Continuous GPS Surveys

Continuously running GPS stations were installed on the glacier surface and in the proglacial area between March and August 2003 and between May and August 2004. Their location is indicated in Figure C.1.

The GPS stations on the ice were processed against "Taku Base", a base station outside the push moraine area. The coordinates for this base station were determined by baseline processing against "Meng", a survey marker on bedrock near the Mendenhall Glacier visitor center in Juneau. "Taku Base" was only instrumented during field campaigns. For other periods, the continuous measurements on the glacier were processed against the continuously running station on the sediments, whose coordinates were determined with respect to "Taku Base". The horizontal displacement of the sediments of about 10 cm over a 5-month-period (Figure C.4) is small compared to the glacier movement and can be neglected for the evaluation of ice velocities. The following coordinates were used for baseline processing (WGS84, UTM zone 8, elevation in ellipsoid height):

1. TakuBase: 6474760.977 556403.235 9.41m (northing-easting-HAE)
2. GPS2003_sed: 6475025.358 556527.757 18.69m (northing-easting-HAE)
3. GPS2004_sed: 6475130.439 556643.191 19.69m (northing-easting-HAE).

The positions of the continuous GPS on the glacier were measured on the half hour, the horizontal velocities calculated for a 24-hour-time interval. The diurnal variations were eliminated with this method. The half-hourly positions of the continuous GPS on the glacier can be found on the data CD (see appendix G). The daily velocities are shown in Figure C.2 and C.3.

The daily positions of the GPS stations on the sediments were determined using the GIPSY/OASIS II GOA4 software (detailed information in section 2.4.1). The complete files with positions relative to Whitehorse (Canada), to Gustavus and relative to the geocenter can be found on the data CD (Appendix G). Figure C.4 shows the daily positions for 2003, Figure C.5 the daily positions 2004, both relative to Whitehorse. For more precise vertical positions of the sediments the data file with positions relative to the geocenter should be used (TK03pfiles.txt and TK04pfiles.txt on CD).

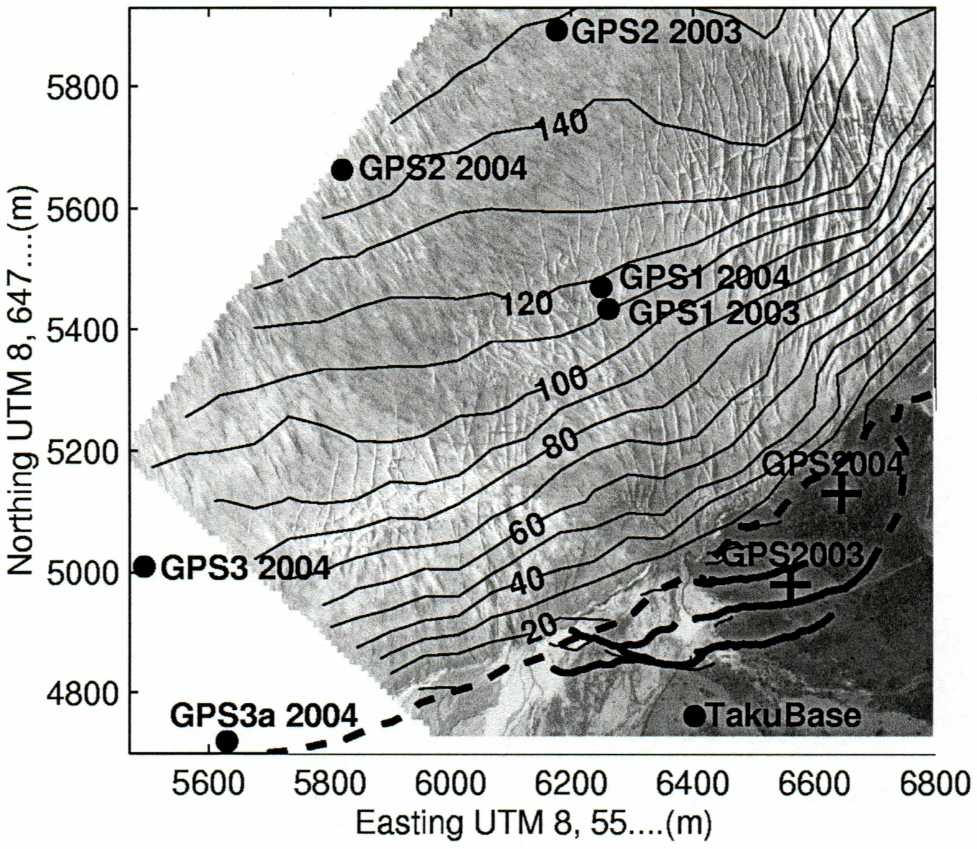

Figure C.1. Location of continuous GPS 2003 and 2004. Between March and August 2003 two continuously running GPS stations were installed on the glacier surface (GPS1 2003, GPS2 2003), three stations were running between May and August 2004 (GPS1 2004, GPS2 2004, GPS3 2004). GPS3 was located very close to the terminus for about two weeks in May and subsequently replaced upglacier for the summer months. The contour lines indicate the glacier surface topography in meters (HAE), the dashed line shows the glacier terminus 2004. The background shows the 2002 Orthophoto. The location of the continuously running GPS stations on the sediments is indicated (GPS2003, GPS2004), as is the location for the base station which was used for baseline processing (TakuBase).

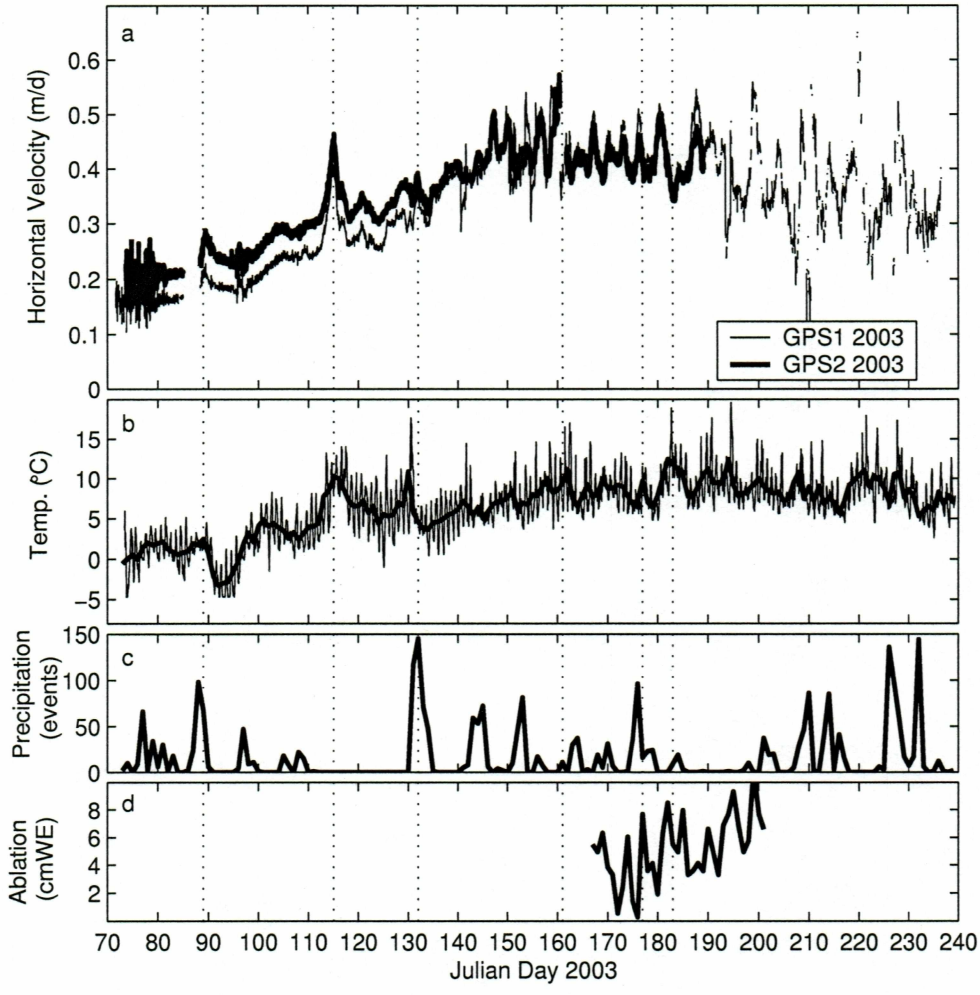

Figure C.2. Continuous GPS 2003 on glacier surface. (a) Daily horizontal velocity, (b) air temperature including mean daily air temperature measured in the proglacial area, (c) daily precipitation in the proglacial area as number of events and (d) mean daily ablation measured on the glacier surface. Due to the increase in instability of the GPS antennas caused by ablation, the velocities became noisier during the summer.

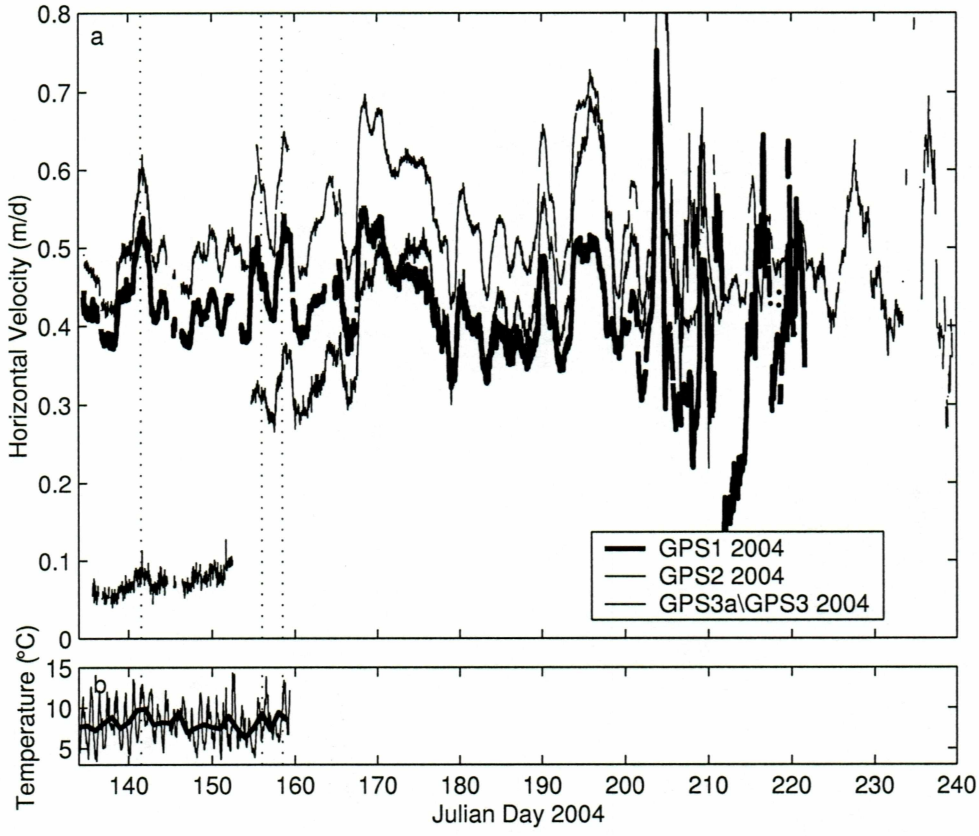

Figure C.3. Continuous GPS 2004 on glacier surface. (a) Daily horizontal velocity, (b) air temperature including mean daily air temperature measured in the proglacial area. Due to the increase in instability of the GPS antennas caused by ablation, the velocities became noisier during the summer.

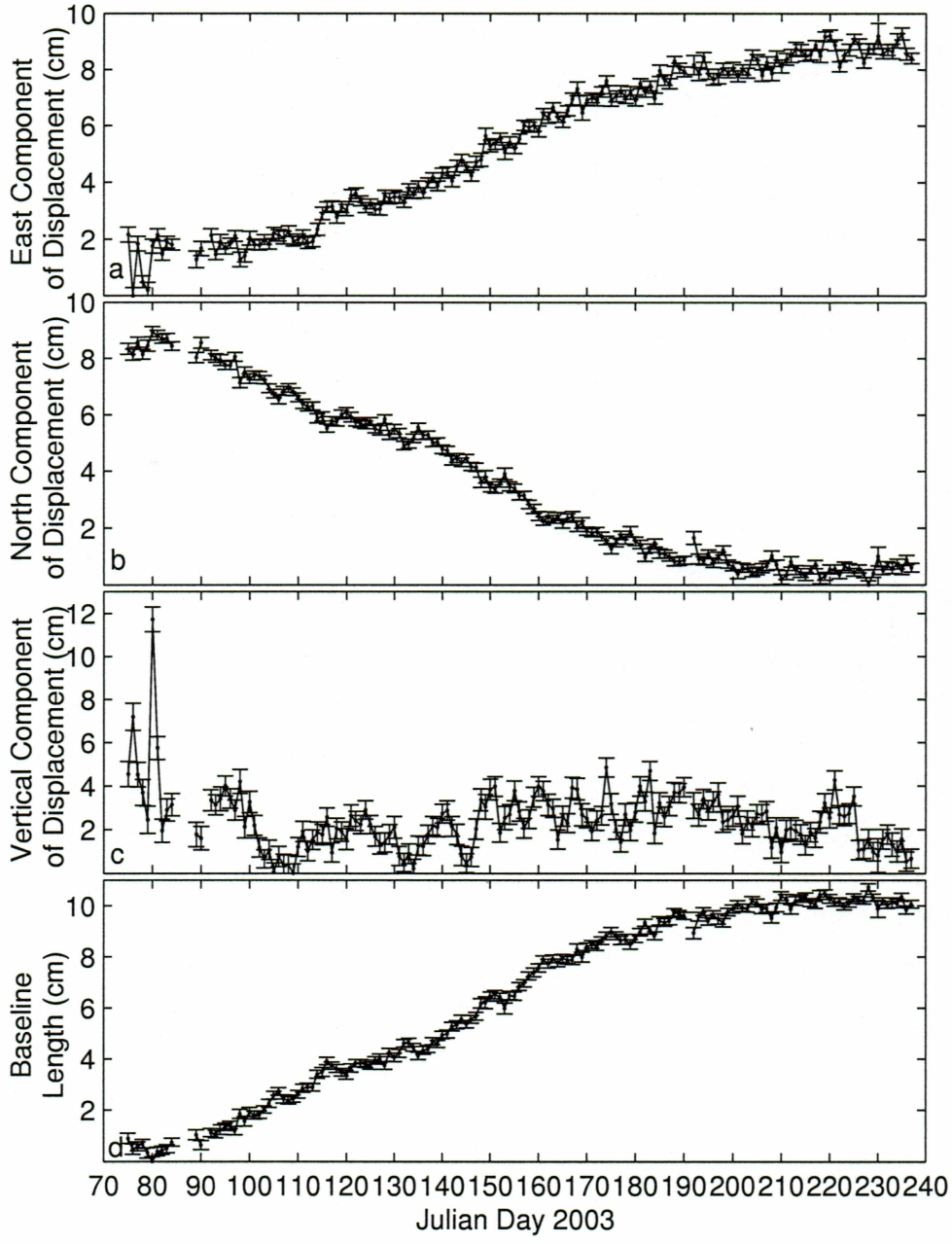

Figure C.4. Continuous GPS 2003 on proglacial sediments. Daily positions of the GPS station "GPS2003" are shown. The positions are relative to a benchmark in Whitehorse. The displacements are shown with respect to an arbitrary point of origin: (a) east component, (b) north component, (c) vertical component and (d) baseline length. The vertical lines show the error range.

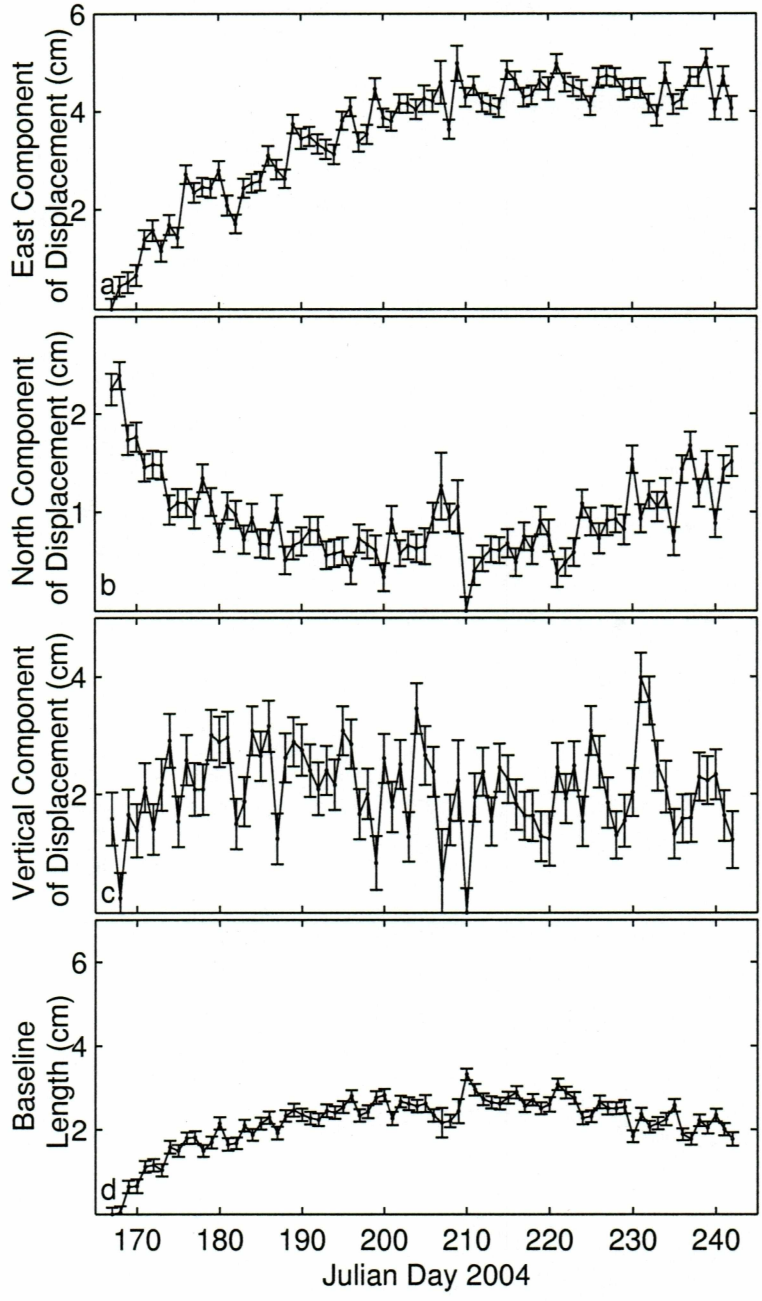

Figure C.5. Continuous GPS 2004 on proglacial sediments. Daily position of the GPS station "GPS2004" are shown. The position is relative to a benchmark in Whitehorse: (a) east component, (b) north component, (c) vertical component and (d) baseline length. The vertical lines show the error range.

Appendix D

Survey Markers on the Glacier Ice

Between fall 2002 and fall 2004 survey markers were installed repeatedly on the glacier surface. We drilled 15-m-deep holes with a steam drill and lowered a stiff wire into the hole. Due to the high summer ablation rate in the area, this method was more efficient than using poles as survey markers. We have measured the location of these wires with precision GPS twice a year. The length of the wire sticking out of the ice provided information about the ablation and the vertical position. The measured coordinate positions and wire lengths are listed in Table D.1. The data are also included in the data CD (Appendix G).

Table D.1: Survey markers on the glacier surface. The naming of the different points is as follows: First part refers to name, second part to month when drilled, third part to Julian-Day of the corresponding year. E.g. "FIIK1_june04_158" is point "FIIK1", drilled in June 2004 and measured on Julian Day 158. FIIK1_june04_241 was measured ~ 1 m east of true location. FIIK7_may04_241, Belly_june03_242, 1choli_241 and 2choli_241 were measured at the end of the wire because the wire has melted out completely. The coordinate system is WGS84, UTM zone8, the elevation is ellipsoid height (HAE).

Name	Date	Julian Day	Northing (m)	Easting (m)	HAE (m)	Wire(m)
FIIK1_aug02	31 Aug 2002	37499.51	6475237.611	556145.629	85.55	NaN
FIIK1_aug02	11 Jun 2003	37783.57	6475186.337	556170.297	75.13	10.75
FIIK1_june03	14 Jun 2003	37786.77	6475177.056	556182.539	71.99	2.28
FIIK1_june03	26 Aug 2003	37859.55	6475151.378	556196.762	66.06	7.99
FIIK1_june03_147	26 May 2004	38133.59	6475113.76	556211.71	63.74	13.7
FIIK1_june03_151	30 May 2004	38137.53	6475112.533	556212.256	63.54	13.93
FIIK1_june03_154	2 Jun 2004	38140.41	6475111.616	556212.67	63.45	14.17
FIIK1_june04_158	6 Jun 2004	38144.52	6475134.8	556196.707	66.90	4.3
FIIK1_june04_241	28 Aug 2004	38227.61	6475108.082	556210.324	61.12	12.92
FIIK2_aug02	31 Aug 2002	37499.53	6475223.019	556418.012	63.44	NaN
FIIK2_aug02	11 Jun 2003	37783.79	6475180.467	556443.489	61.68	7.89
FIIK2_june03	14 Jun 2003	37786.79	6475179.571	556444.108	61.52	0.99
FIIK2_june03	26 Aug 2003	37859.66	6475162.326	556456.756	57.78	7.11
FIIK2_may04_150	29 May 2004	38136.5	6475355.815	556410.903	83.47	0.51

Table D.1: Continued

Name	Date	Julian Day	Northing (m)	Easting (m)	HAE (m)	Wire (m)
FIIK2_may04_243	30 Aug 2004	38229.44	6475333.244	556427.256	78.02	7.45
FIIK3_aug02	31 Aug 2002	37499.44	6475540.953	556167.632	116.52	NaN
FIIK3_aug02_159	8 Jun 2003	37780.68	6475488.268	556195.238	117.23	5.4
FIIK3_aug02_162	11 Jun 2003	37783.76	6475486.865	556196.007	117.04	5.76
FIIK3_aug02	26 Aug 2003	37859.63	6475460.752	556210.875	113.42	11.27
FIIK3_aug03	28 Aug 2003	37861.46	6475461.027	556208.397	113.49	3.45
FIIK3_aug03_150	29 May 2004	38136.51	6475412.439	556234.12	111.69	7.84
FIIK3_may04_150	29 May 2004	38136.55	6475536.72	556190.844	125.15	0.35
FIIK3_may04_241	28 Aug 2004	38227.57	6475506.92	556208.07	121.03	7.52
FIIK4_aug02	31 Aug 2002	37499.48	6475500.16	556387.747	102.86	NaN
FIIK4_aug02	11 Jun 2003	37783.78	6475447.426	556416.287	95.25	6.36
FIIK4_aug02	26 Aug 2003	37859.64	6475427.054	556430.328	87.93	12.74
FIIK4_aug03	28 Aug 2003	37861.48	6475525.743	556372.572	111.62	0.2
FIIK4_aug03_144	23 May 2004	38130.5	6475476.855	556398.646	107.01	4.1
FIIK4_aug03_241	28 Aug 2004	38227.56	6475450.28	556416.111	97.38	12.86
FIIK5_aug02	31 Aug 2002	37499.46	6475920.535	556521.627	135.97	NaN
FIIK5_aug02	10 Jun 2003	37782.65	6475863.968	556560.766	136.60	5.52
FIIK5_june03	14 Jun 2003	37786.81	6475928.21	556530.231	140.41	0.72
FIIK5_june03	26 Aug 2003	37859.6	6475909.252	556543.406	136.77	6.44
FIIK5_june03_148	27 May 2004	38134.55	6475855.428	556583.475	138.50	10.5
FIIK5_may04_150	29 May 2004	38136.64	6476021.136	556480.374	145.85	0.63
FIIK5_may04_241	28 Aug 2004	38227.53	6475996.86	556497.438	137.59	9.5
FIIK6_aug02	31 Aug 2002	37499.39	6474985.121	555668.27	73.68	NaN
FIIK6_aug02_162	11 Jun 2003	37783.41	6474938.374	555682.444	69.88	6.08
FIIK6_aug02_165	14 Jun 2003	37786.75	6474936.45	555683.115	69.60	NaN
FIIK6_aug02_238	26 Aug 2003	37859.53	6474894.694	555696.849	60.07	14.32
FIIK6_aug02_240	28 Aug 2003	37861.4	6474896.281	555698.877	63.31	NaN
FIIK6_aug03	28 Aug 2003	37861.42	6474974.459	555682.387	76.24	1.4
FIIK6_aug03_150	29 May 2004	38136.67	6474945.827	555691.142	73.17	6.12
FIIK6_aug03_163	11 Jun 2004	38149.73	6474942.323	555692.27	72.31	7.1

Table D.1: Continued

Name	Date	Julian Day	Northing (m)	Easting (m)	HAE (m)	Wire (m)
FIIK6_june04_163	11 Jun 2004	38149.76	6474940.441	555689.452	72.43	3.2
FIIK6_june04_241	28 Aug 2004	38227.4	6474910.869	555700.071	65.32	10.48
FIIK7_may04_144	23 May 2004	38130.44	6475610.454	556888.367	51.37	0.05
FIIK7_may04_148	27 May 2004	38134.65	6475609.482	556889.458	50.86	0.45
FIIK7_may04_154	2 Jun 2004	38140.64	6475608.087	556891.002	50.21	0.96
FIIK7_may04_158	6 Jun 2004	38144.79	6475607.146	556892.12	49.61	1.35
FIIK7_may04_161	9 Jun 2004	38147.63	6475606.486	556892.892	49.20	1.8
FIIK7_may04_241	28 Aug 2004	38227.4	6475592.889	556909.256	37.81	9.5
FIIK8_may04_147	26 May 2004	38133.66	6474987.365	555923.059	61.88	0.75
FIIK8_may04_149	28 May 2004	38135.57	6474986.913	555923.221	61.62	0.89
FIIK8_may04_151	30 May 2004	38137.55	6474986.276	555923.409	61.57	0.91
FIIK8_may04_153	1 Jun 2004	38139.67	6474985.674	555923.617	61.43	1.18
FIIK8_may04_157	5 Jun 2004	38143.76	6474984.386	555924.1	61.17	1.42
FIIK8_may04_164	12 Jun 2004	38150.5	6474982.123	555924.924	60.65	2
FIIK8_may04_241	28 Aug 2004	38227.39	6474954.065	555936.762	53.00	10.2
FIIK9_may04_149	28 May 2004	38135.48	6476251.376	556849.228	136.19	0.9
FIIK9_may04_154	2 Jun 2004	38140.61	6476250.113	556850.465	135.99	1.27
FIIK9_may04_161	9 Jun 2004	38147.61	6476248.389	556852.232	135.73	1.78
FIIK9_may04_241	28 Aug 2004	38227.43	6476234.271	556866.174	130.74	8.54
JIRP_wheel	31 Aug 2002	37499.46	6475834.219	556367.611	128.99	NaN
JIRP_wheel	10 Jun 2003	37782.69	6475778.516	556400.681	131.59	NaN
JIRP_wheel	26 Aug 2003	37859.59	6475757.519	556413.883	128.66	NaN
GPS_upper	26 Aug 2003	37859.58	6475843.21	556201.845	133.06	8.83
GPSup_aug03_150	29 May 2004	38136.62	6475786.866	556233.501	134.02	11.3
GPSup_may04_150	29 May 2004	38136.62	6475786.866	556233.501	134.02	3.18
GPSup_may04_154	2 Jun 2004	38140.52	6475785.548	556234.248	133.92	3.42
GPSup_may04_161	9 Jun 2004	38147.53	6475783.129	556235.811	133.60	3.92
GPSup_may04_241	28 Aug 2004	38227.46	6475760.484	556249.396	128.93	9.97
TermRad_june03	10 Jun 2003	37782.51	6476972.055	556072.382	197.17	1.36
TermRad_june03	27 Aug 2003	37860.68	6476949.55	556107.755	194.18	5.45
TermRad_june03_152	31 May 2004	38138.51	6476886.536	556215.359	198.47	8.19
TermRad_may04_152	31 May 2004	38138.51	6476886.536	556215.359	198.47	2.85
TermRad_may04_242	29 Aug 2004	38228.4	6476865.048	556249.288	194.05	9

Table D.1: Continued

Name	Date	Julian Day	Northing (m)	Easting (m)	HAE (m)	Wire (m)
Belly_june03	9 Jun 2003	37781.78	6478370.389	555068.646	271.23	1.46
Belly_june03	27 Aug 2003	37860.5	6478333.122	555124.026	263.33	5.61
Belly_june03_242	29 Aug 2004	38228.44	6478195.918	555366.009	251.19	13.92
Belly_june04_161	10 Jun 2004	38148.58	6478393.045	555061.513	269.71	1.25
Belly_june04_242	29 Aug 2004	38228.46	6478358.671	555114.431	261.12	6.81
Bra_june03	9 Jun 2003	37781.53	6479307.799	552866.54	352.99	1.42
Bra_june03	27 Aug 2003	37860.57	6479237.701	552889.115	346.91	5.55
Bra_june03_161	10 Jun 2004	38148.7	6479015.116	552972.93	344.36	7.3
Bra_june04_161	10 Jun 2004	38148.7	6479015.116	552972.93	344.36	0.05
Bra_june04_242	29 Aug 2004	38228.52	6478952.683	552998.71	337.99	4.93
1trough_145	24 May 2004	38131.48	6476209.765	555996.954	168.22	0.62
1trough_148	27 May 2004	38134.59	6476208.555	555997.762	168.02	0.76
1trough_154	2 Jun 2004	38140.54	6476206.211	555999.39	167.70	1.14
1trough_161	9 Jun 2004	38147.54	6476203.195	556001.399	167.18	1.65
1trough_241	28 Aug 2004	38227.51	6476176.508	556018.218	160.55	9.5
2trough_145	24 May 2004	38131.62	6476207.559	556326.409	160.95	0.61
2trough_148	27 May 2004	38134.61	6476206.55	556327.14	160.86	0.72
2trough_154	2 Jun 2004	38140.56	6476204.496	556328.615	160.67	1.09
2trough_158	6 Jun 2004	38144.56	6476203.036	556329.663	160.51	0.36
2trough_161	9 Jun 2004	38147.56	6476201.934	556330.449	160.36	0.56
2trough_241	28 Aug 2004	38227.48	6476180.316	556345.559	154.58	8.61
3trough_148	27 May 2004	38134.63	6476280.297	556547.693	164.20	−1.4
3trough_154	2 Jun 2004	38140.58	6476278.526	556549.372	163.77	0.32
3trough_161	9 Jun 2004	38147.58	6476276.304	556551.415	163.16	1.02
1choli_144	23 May 2004	38130.48	6475300.396	556653.475	37.36	1.35
1choli_148	27 May 2004	38134.7	6475299.704	556654.176	37.13	1.78
1choli_154	2 Jun 2004	38140.69	6475298.701	556655.169	36.96	2.21
1choli_157	5 Jun 2004	38143.62	6475298.182	556655.72	36.86	2.54
1choli_161	9 Jun 2004	38147.49	6475297.512	556656.388	36.43	3.3
1choli_241	28 Aug 2004	38227.53	6475287.37	556667.392	30.57	10.41
2choli_144	23 May 2004	38130.46	6475415.138	556739.114	48.55	0.8
2choli_148	27 May 2004	38134.68	6475414.107	556740.061	48.14	1.24

Table D.1: Continued

Name	Date	Julian Day	Northing (m)	Easting (m)	HAE (m)	Wire (m)
2choli_154	2 Jun 2004	38140.67	6475412.55	556741.377	47.52	1.74
2choli_157	5 Jun 2004	38143.64	6475411.715	556742.072	47.26	2.06
2choli_161	9 Jun 2004	38147.47	6475410.716	556742.979	46.69	2.56
2choli_241	28 Aug 2004	38227.51	6475394.053	556756.254	36.73	10.15
1sun_147	26 May 2004	38133.69	6474887.525	555953.662	41.49	0.66
1sun_149	28 May 2004	38135.56	6474887.098	555953.763	41.35	0.79
1sun_151	30 May 2004	38137.56	6474886.576	555953.924	41.17	0.81
1sun_153	1 Jun 2004	38139.69	6474886.014	555954.035	40.97	NaN
1sun_157	5 Jun 2004	38143.75	6474884.873	555954.363	40.63	1.48
1sun_164	12 Jun 2004	38150.48	6474882.746	555954.986	39.88	2.23
2sun_147	26 May 2004	38133.71	6474824.341	555985.951	20.23	0.49
2sun_149	28 May 2004	38135.55	6474823.987	555986.025	20.14	0.65
2sun_151	30 May 2004	38137.57	6474823.486	555986.104	19.97	0.78
2sun_153	1 Jun 2004	38139.7	6474823	555986.253	19.79	NaN
2sun_157	5 Jun 2004	38143.73	6474821.918	555986.491	19.49	1.39
2sun_164	12 Jun 2004	38150.51	6474819.996	555986.978	18.91	2.12
TakuBase	13 Jun 2004		6474760.977	556403.235	9.41	NaN
GPS2003_sed			6475025.358	556527.757	18.69	NaN
GPS2004_sed			6475130.439	556643.191	19.69	NaN

Appendix E

Survey Markers on the Proglacial Sediments

Multiple survey markers were established on the proglacial area between 2002 and 2004. They were measured twice a year, in early June and late August of the corresponding years. Precsion GPS receivers were used and the baselines were processed against the fixed base station "TakuBase". The horizontal error in baseline length is 6 mm except for the markers along line E (EA to EF) where it amounts to 1.1 cm due to a less precise positioning of the GPS antenna. The vertical error is about 2.3 cm. The location of all markers including the naming is shown in Figure E.1. The coordinate positions (WGS84, UTM zone 8, ellipsoid height HAE) are given in Tables E.1 to E.5.

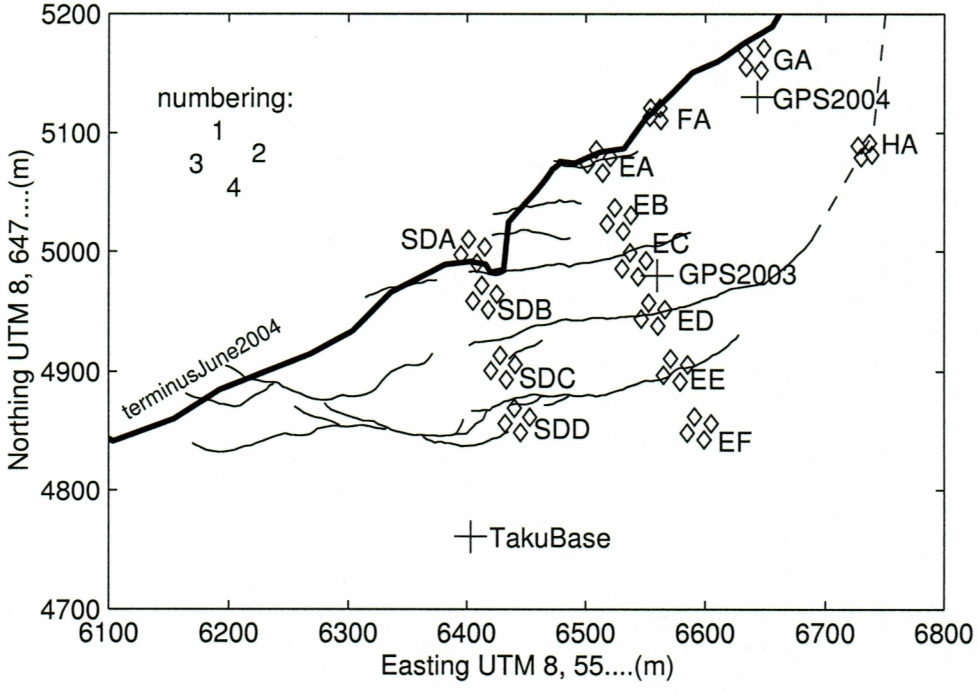

Figure E.1. Location map of survey markers in the proglacial area. The diamonds represent all markers that were repeatedly measured between 2002 and 2004. "GPS2003" and "GPS2004" show the location of the continuously running GPS stations on the sediments (Appendix C). The markers are labeled and numbered as used in the following tables.

Table E.1: Survey markers on proglacial sediments August 2002. Location of the survey markers is shown in Figure E.1. The coordinate system is WGS84, UTM zone8, the elevation is ellipsoid height (HAE).

Name	Date	Julian Day	Northing (m)	Easting (m)	HAE (m)
SDA1	31 Aug 2002	243.56	6475010.44	556401.562	21.46
SDA2	31 Aug 2002	243.57	6475003.9	556415.015	21.63
SDA3	31 Aug 2002	243.57	6474997.285	556395.117	21.60
SDA4	31 Aug 2002	243.58	6474990.496	556408.43	21.60
EA1	31 Aug 2002	243.59	6475086.745	556507.758	23.62
EA2	31 Aug 2002	243.6	6475079.206	556520.422	23.95
EA3	31 Aug 2002	243.6	6475073.566	556501.222	24.26
EA4	31 Aug 2002	243.61	6475066.14	556514.012	22.49
EB1	31 Aug 2002	243.62	6475036.948	556524.252	20.63
EB2	31 Aug 2002	243.62	6475030.725	556537.848	20.93
EB3	31 Aug 2002	243.63	6475023.571	556517.659	21.40
EB4	31 Aug 2002	243.64	6475017.228	556531.248	21.43
EC1	31 Aug 2002	243.64	6474999.224	556537.202	19.24
EC2	31 Aug 2002	243.65	6474992.51	556550.567	19.25
EC3	31 Aug 2002	243.65	6474985.904	556530.438	19.32
EC4	31 Aug 2002	243.66	6474979.337	556543.933	18.95
ED1	31 Aug 2002	243.67	6474957.194	556552.82	15.19
ED2	31 Aug 2002	243.67	6474951.766	556566.353	11.25
ED3	31 Aug 2002	243.68	6474943.972	556546.688	10.89
ED4	31 Aug 2002	243.68	6474938.089	556560.475	11.08
EE1	31 Aug 2002	243.7	6474910.835	556571.185	10.45
EE2	31 Aug 2002	243.7	6474905.681	556585.256	9.44
EE3	31 Aug 2002	243.71	6474896.963	556565.248	9.95
EE4	31 Aug 2002	243.72	6474891.441	556579.107	8.93
EF1	31 Aug 2002	243.74	6474862.304	556591.074	8.70
EF2	31 Aug 2002	243.75	6474856.592	556604.953	8.54
EF3	31 Aug 2002	243.76	6474848.556	556585.035	8.63
EF4	31 Aug 2002	243.76	6474842.824	556598.971	8.57
TakuBase	31 Aug 2002	243.38	6474760.977	556403.235	9.41

Table E.2: Survey markers on proglacial sediments June 2003. Location of the survey markers is shown in Figure E.1. The coordinate system is WGS84, UTM zone8, the elevation is ellipsoid height (HAE).

Name	Date	Julian Day	Northing (m)	Easting (m)	HAE (m)
EA1	6/14/2003	165.5	6475085.675	556508.648	23.61
EA2	6/14/2003	165.52	6475079.041	556520.512	23.77
EA3	6/14/2003	165.51	6475073.466	556501.31	24.18
EA4	6/14/2003	165.53	6475066.019	556514.099	22.33
EB1	6/10/2003	161.53	6475036.855	556524.316	20.53
EB2	6/10/2003	161.52	6475030.648	556537.913	20.81
EB3	6/10/2003	161.52	6475023.478	556517.752	21.28
EB4	6/10/2003	161.51	6475017.146	556531.3	21.27
EC1	6/10/2003	161.49	6474999.174	556537.243	19.10
EC4	6/10/2003	161.48	6474979.274	556543.981	18.79
ED1	6/10/2003	161.48	6474957.162	556552.853	15.08
ED4	6/10/2003	161.46	6474938.088	556560.489	10.99
EE1	6/15/2003	166.46	6474910.828	556571.196	10.34
EE4	6/15/2003	166.47	6474891.431	556579.142	8.86
EF4	6/15/2003	166.49	6474842.828	556598.987	8.48
FA1	6/12/2003	163.68	6475121.396	556553.867	24.75
FA2	6/12/2003	163.7	6475120.574	556562.007	24.33
FA3	6/12/2003	163.72	6475113.299	556553.675	24.05
FA4	6/12/2003	163.73	6475110.446	556562.643	23.49
GA1	6/14/2003	165.75	6475169.21	556632.975	24.55
GA2	6/14/2003	165.76	6475171.392	556648.455	23.27
GA3	6/14/2003	165.75	6475155.08	556633.592	24.26
GA4	6/14/2003	165.76	6475152.697	556646.11	22.44
HA1	6/15/2003	166.43	6475088.891	556726.991	7.48
HA2	6/15/2003	166.44	6475091.168	556736.795	7.33
HA3	6/15/2003	166.44	6475079.116	556729.733	7.46
HA4	6/15/2003	166.45	6475081.262	556738.785	7.39
SDA2	6/14/2003	165.54	6475003.796	556415.052	21.47
SDA4	6/8/2003	159.84	6474990.439	556408.474	21.46
SDB1	6/9/2003	160.44	6474971.733	556412.655	19.95
SDB2	6/9/2003	160.45	6474964.345	556425.637	19.26
SDB3	6/9/2003	160.46	6474958.824	556405.141	18.93
SDB4	6/9/2003	160.47	6474951.432	556418.12	18.11
SDC1	6/9/2003	160.57	6474913.512	556428.295	13.09
SDC2	6/9/2003	160.62	6474905.898	556441.167	13.33
SDC3	6/9/2003	160.63	6474900.721	556420.511	13.25
SDC4	6/9/2003	160.64	6474893.1	556433.415	13.35

Table E.2: Continued

Name	Date	Julian Day	Northing (m)	Easting (m)	HAE (m)
SDD1	6/9/2003	160.65	6474869.371	556440.273	10.10
SDD2	6/9/2003	160.66	6474861.846	556453.147	9.68
SDD3	6/9/2003	160.67	6474856.539	556432.534	10.13
SDD4	6/9/2003	160.68	6474849.016	556445.454	9.75
TakuBase			6474760.977	556403.235	9.41
GPS2003_sed			6475025.358	556527.757	18.69

Table E.3: Survey markers on proglacial sediments August 2003. Location of the survey markers is shown in Figure E.1. The coordinate system is WGS84, UTM zone8, the elevation is ellipsoid height (HAE).

Name	Date	Julian Day	Northing (m)	Easting (m)	HAE (m)
EA1	26 Aug 2003	238.74	6475085.625	556508.72	23.54
EA2	26 Aug 2003	238.73	6475079.047	556520.556	23.74
EA3	26 Aug 2003	238.73	6475073.432	556501.36	24.18
EA4	26 Aug 2003	238.73	6475066.015	556514.14	22.38
EB1	26 Aug 2003	238.72	6475036.832	556524.354	20.53
EB2	26 Aug 2003	238.71	6475030.613	556537.942	20.82
EB3	26 Aug 2003	238.71	6475023.429	556517.767	21.29
EB4	26 Aug 2003	238.71	6475017.107	556531.323	21.29
EC1	26 Aug 2003	238.7	6474999.125	556537.247	19.13
EC4	26 Aug 2003	238.69	6474979.251	556543.995	18.77
ED1	26 Aug 2003	238.68	6474957.134	556552.856	15.08
ED4	26 Aug 2003	238.67	6474938.077	556560.484	10.99
EE1	26 Aug 2003	238.65	6474910.783	556571.204	10.32
EE4	26 Aug 2003	238.65	6474891.406	556579.136	8.85
EF4	26 Aug 2003	238.64	6474856.59	556604.951	8.47
FA1	26 Aug 2003	238.76	6475120.827	556554.33	24.67
FA2	26 Aug 2003	238.75	6475120.552	556562.067	24.38
FA3	26 Aug 2003	238.77	6475113.285	556553.763	24.09
FA4	26 Aug 2003	238.78	6475110.439	556562.73	23.53
GA1	26 Aug 2003	238.75	6475169.203	556632.985	24.53
GA2	26 Aug 2003	238.76	6475171.371	556648.496	23.28
GA3	26 Aug 2003	238.74	6475155.083	556633.628	24.24
GA4	26 Aug 2003	238.75	6475152.667	556646.159	22.40
HA1	26 Aug 2003	238.78	6475088.86	556727.028	7.51
HA2	26 Aug 2003	238.77	6475091.141	556736.814	7.35
HA3	26 Aug 2003	238.79	6475079.091	556729.765	7.52
HA4	26 Aug 2003	238.79	6475081.267	556738.812	7.45

Table E.3: Continued

Name	Date	Julian Day	Northing (m)	Easting (m)	HAE (m)
SDA2	27 Aug 2003	239.53	6475003.795	556415.062	21.51
SDA4	27 Aug 2003	239.52	6474990.39	556408.471	21.47
SDB1	27 Aug 2003	239.54	6474971.713	556412.667	19.80
SDB2	27 Aug 2003	239.54	6474964.34	556425.643	19.31
SDB3	27 Aug 2003	239.55	6474958.806	556405.14	18.92
SDB4	27 Aug 2003	239.56	6474951.429	556418.135	18.11
SDC1	26 Aug 2003	238.56	6474913.497	556428.313	13.14
SDC2	26 Aug 2003	238.57	6474905.896	556441.178	13.37
SDC3	26 Aug 2003	238.58	6474900.683	556420.524	13.34
SDD1	26 Aug 2003	238.6	6474869.388	556440.282	10.16
SDD2	26 Aug 2003	238.61	6474861.846	556453.139	9.69
SDD3	26 Aug 2003	238.62	6474856.542	556432.524	10.23
SDD4	26 Aug 2003	238.62	6474849.007	556445.443	9.79
TakuBase			6474760.977	556403.235	9.41
GPS2003_sed			6475025.358	556527.757	18.69

Table E.4: Survey markers on proglacial sediments May/June 2004. Location of the survey markers is shown in Figure E.1. The coordinate system is WGS84, UTM zone8, the elevation is ellipsoid height (HAE).

Name	Date	Julian Day	Northing (m)	Easting (m)	HAE (m)
EA3	13 May 2004	134.43	6475073.327	556501.404	24.04
EA4	13 May 2004	134.51	6475065.882	556514.191	22.33
EB1	13 May 2004	134.52	6475036.759	556524.386	20.53
EB2	13 May 2004	134.52	6475030.542	556537.981	20.82
EB3	13 May 2004	134.54	6475023.368	556517.797	21.24
EB4	13 May 2004	134.53	6475017.035	556531.358	21.28
SDB1	13 May 2004	134.55	6474971.651	556412.71	19.79
SDB2	13 May 2004	134.56	6474964.266	556425.693	19.32
SDB3	13 May 2004	134.56	6474958.735	556405.2	18.95
SDB4	13 May 2004	134.57	6474951.346	556418.177	18.14
FA2	15 May 2004	136.51	6475118.63	556563.653	24.49
FA2	7 Jun 2004	159.57	6475117.513	556564.794	24.50
FA3	15 May 2004	136.52	6475110.674	556556.251	23.70
FA4	15 May 2004	136.54	6475110.132	556563.031	23.36
FA4	7 Jun 2004	159.6	6475110.098	556563.081	23.39
GA_center	13 May 2004	134.64	6475163.388	556640.177	24.13
GA_center	13 Jun 2004	165.58	6475163.369	556640.233	24.12
GA3	13 May 2004	134.65	6475155.022	556633.712	24.23

Table E.4: Continued

Name	Date	Julian Day	Northing (m)	Easting (m)	HAE (m)
GA3	13 Jun 2004	165.6	6475155.006	556633.754	24.25
GA4	13 May 2004	134.67	6475152.618	556646.242	22.44
GA4	13 Jun 2004	165.61	6475152.614	556646.285	22.46
TakuBase	13 Jun 2004	165.39	6474760.977	556403.235	9.41
GPS2004_sed			6475130.439	556643.191	19.69

Table E.5: Survey markers on proglacial sediments August 2004. Location of the survey markers is shown in Figure E.1. The coordinate system is WGS84, UTM zone8, the elevation is ellipsoid height (HAE).

Name	Date	Julian Day	Northing (m)	Easting (m)	HAE (m)
GA_center	30 Aug 2004	243.52	6475163.364	556640.276	24.13
GA3	30 Aug 2004	243.53	6475154.988	556633.813	24.24
GA4	30 Aug 2004	243.55	6475152.591	556646.338	22.45
EA3	30 Aug 2004	243.61	6475073.247	556501.48	24.04
EA4	30 Aug 2004	243.63	6475065.818	556514.278	22.31
SDB1	30 Aug 2004	243.67	6474971.618	556412.748	19.83
SDB2	30 Aug 2004	243.68	6474964.236	556425.726	19.32
SDB3	30 Aug 2004	243.69	6474958.708	556405.241	18.97
SDB4	30 Aug 2004	243.71	6474951.33	556418.216	18.12
TakuBase		165.39	6474760.977	556403.235	9.41
GPS2004_sed			6475130.439	556643.191	19.69

Appendix F
Stable Isotopes

F.1 Background

The constituents of water, oxygen and hydrogen, occur in different isotopes with different atomic masses due to a difference in the number of neutrons. Oxygen has three stable isotopes (^{16}O,^{17} O,^{18} O) and hydrogen has two (^{1}H, ^{2}H deuterium). Isotopic fractionation occurs during chemical precesses like evaporation, condensation and diffusion. Isotopic ratios are given as deviation δ of a given standard ratio, e.g. SMOW (ratio for Standard Mean Ocean Water). Isotopic ratios are given as

$$\delta^{18}O = \frac{(\frac{^{18}O}{^{16}O})_{sample} - (\frac{^{18}O}{^{16}O})_{SMOW}}{(\frac{^{18}O}{^{16}O})_{SMOW}} * 1000 \quad [‰] \tag{F.1}$$

$$\delta^{2}H = \frac{(\frac{^{2}H}{^{1}H})_{sample} - (\frac{^{2}H}{^{1}H})_{SMOW}}{(\frac{^{2}H}{^{1}H})_{SMOW}} * 1000 \quad [‰] \, . \tag{F.2}$$

Heavy isotopes make stronger hydrogen bonds than light isotopes. Therefore, ice is enriched in ^{18}O (^{2}H) and depleted in ^{16}O (^{1}H) compared to the liquid water.

F.2 Ice and Water Samples 2004

Several ice and water samples were taken in the terminal area of Taku Glacier in June 2004. The goal of this study was to investigate if the basal layers observed at the glacier bed along the margin (Figure F.1) derived from refrozen basal meltwater. Subglacial water that is derived from melting of englacial ice has little isotopic fractionation. In an open system, the freezing of subglacial discharge results in basal ice that is isotopically heavier. The samples were collected at ten different sites (see Table F.1) and analyzed at the Alaska Stable Isotope Facility at the University of Alaska Fairbanks (http://www.uaf.edu/water/ASIF/ASIF.html).

The results are summarized in Table F.1 and plotted in Figures F.2, F.3, F.4. These figures show that (1) the sediment rich basal ice has the heaviest isotopic composition (2) the ice becomes isotopically lighter higher above the glacier base. This leads to the conclusion that sediment bearing freeze-on layers presumably derive from water saturated subglacial sediments.

Table F.1. Isotopic composition of ice and water samples. Labeling of the approximate locations follows the naming in Appendix C and G. The elevation is an approximation only. More detailed information is included on the data CD in the back pocket.

Sample Name	$\delta^{18}O$ (‰) SMOW	$\delta^{2}H$ (‰) SMOW	Elevation HAE (m)	type	approx. location
1	-106.22	-13.83	20	sediment rich	below "edmea3/edmea4"
3	-106.89	-14.23	21	clear ice	directly above 1
4	-114.88	-15.39		subglacial water	
5	-111.78	-14.95		supraglacial water	
6	-101.30	-13.47	15	sediment rich	very east end of pm
8	-107.74	-14.28	16	clear ice	directly above 6
12	-107.32	-14.09	55	clear ice	at "edmea5"
13	-115.50	-15.44	105	clear ice	at "GPS1 2004"
14	-121.09	-15.93	140	clear ice	at "GPS2 2004"
15	-156.36	-19.76		rainwater	

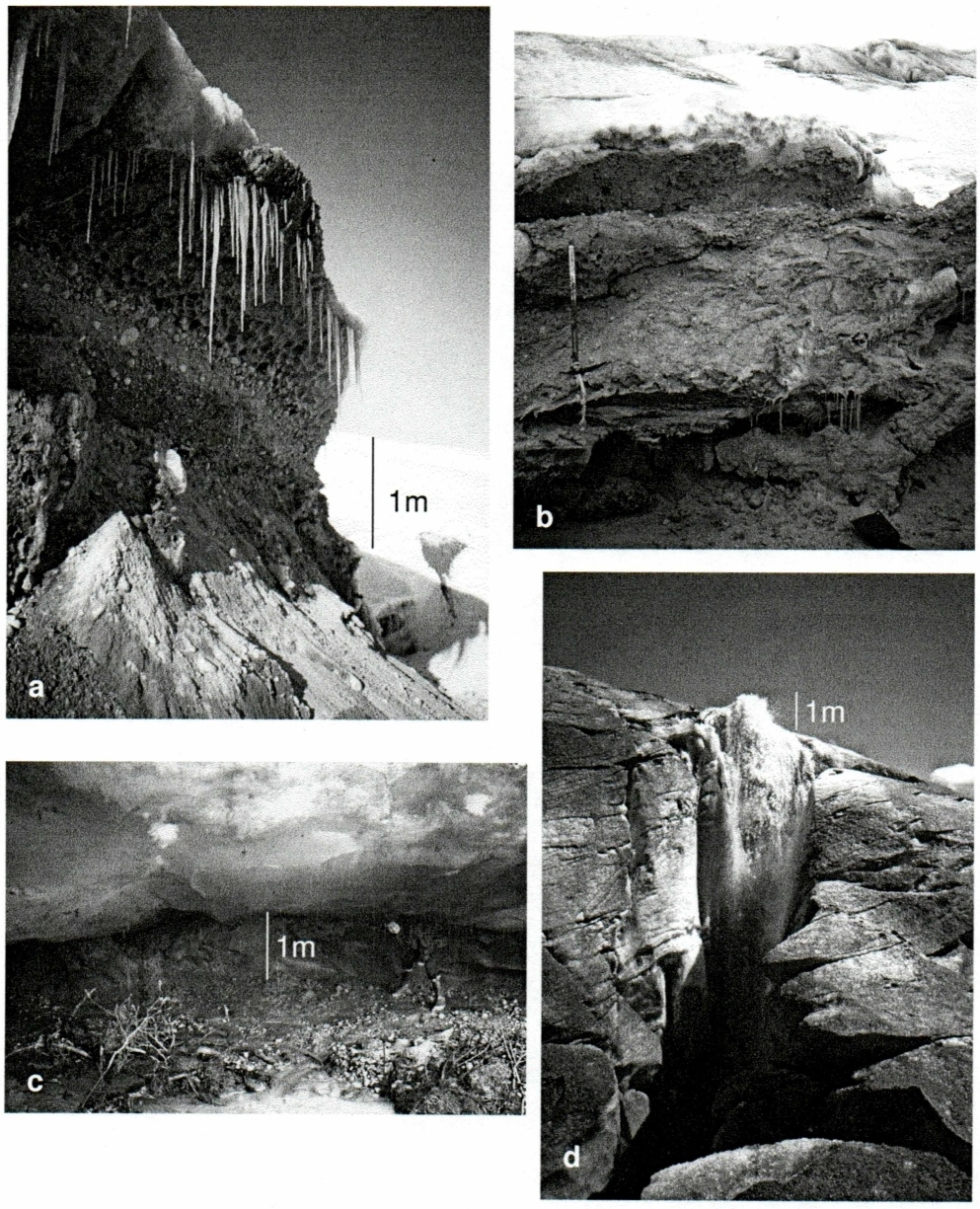

Figure F.1. Freeze-on layers. Sediment-bearing freeze-on layers were observed at different locations at the glacier bed along the terminus (a,b,c). They were about 0.5 to 1 m thick. (a) March 2003: near Site B (Figure 2.2), (b) March 2003: east end of push moraine area, (c) June 2004: east end of push moraine area, (d) June 2003: about 100 m from the terminus an artesian well on the glacier surface froze a fresh "ice cone" about 1 m high. Location $\sim$ 500 m west of push moraine area, west of Site A (Figure 2.2).

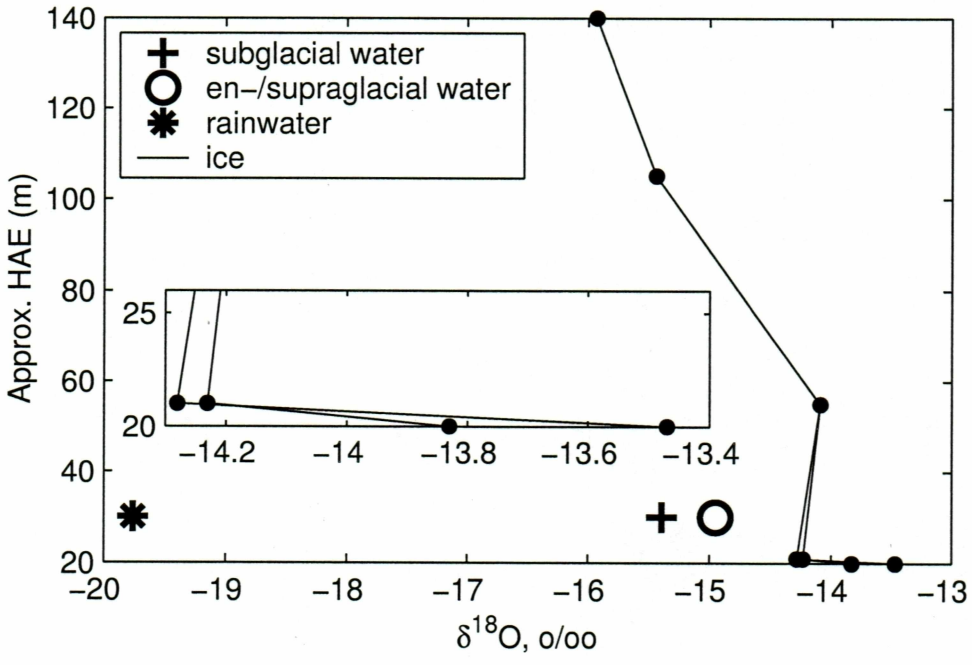

Figure F.2. Oxygen isotopes. Vertical profile of oxygen isotope ratios. The sediment bearing layers at the glacier bed (rectangular inset) were isotopically heavier than the glacier ice above and than any sub-, en- or supraglacial water.

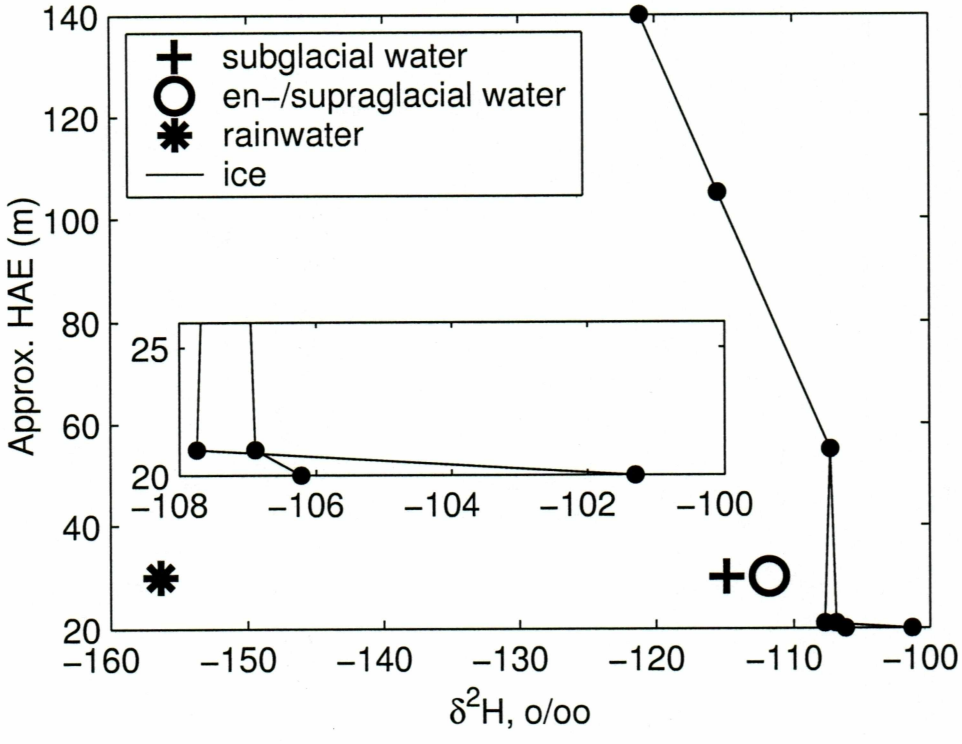

Figure F.3. Hydrogen isotopes. Vertical profile of hydrogen isotope ratios. The sediment bearing layers at the glacier bed (rectangular inset) were isotopically heavier than the glacier ice above and than any sub-, en- or supraglacial water.

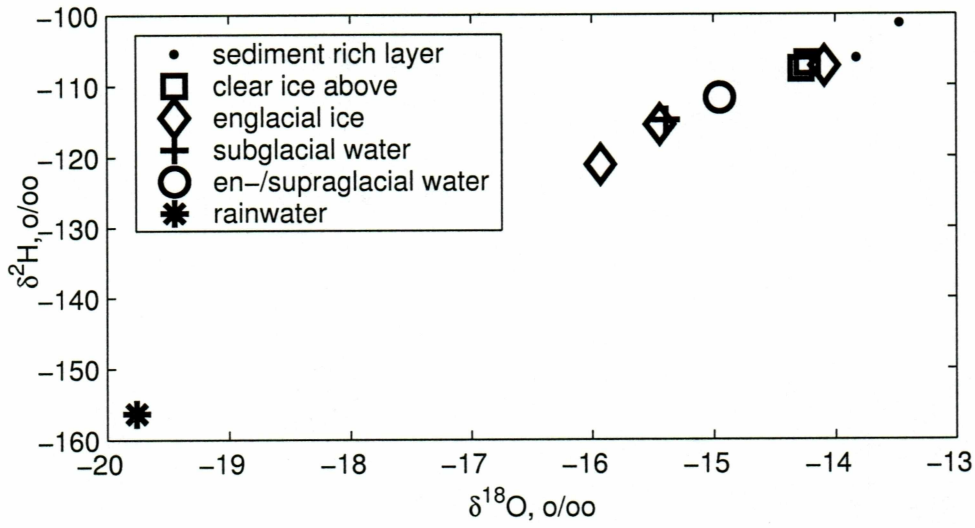

Figure F.4. Co-isotopic composition of basal and englacial water, rainwater and the sediment rich basal layer.

Appendix G

Archived Data

Digital files on the CD-ROM in the pocket at the end of the thesis:

RES folder contents

res_coordinates89_90.txt	Radio-echo soundings 1989/1990
res_coordinates89_90.xls	
Taku Radar Points 89 90.txt	
Taku Radar Points 89 90.xls	
res2003_original.txt	Radio-echo soundings 2003 original data
res2003_summary.txt	RES 2003 including calculated bed elevations
res2004_original.txt	Radio-echo soundings 2004 original data
res2004_summary.txt	RES 2004 including calculated bed elevations
res_2003_2004_summary.txt	see Table B.1 in Appendix B of the thesis
RES_loc_0304_all.tif	Figure with location RES 2003/2004 all
RES_loc_0304_termArea.tif	Figure with location RES 2003/2004 terminal area
Readme_RES.txt	

Continuous GPS (glacier) folder contents

GPS1_2003.txt	Daily positions GPS1 2003
GPS2_2003.txt	Daily positions GPS2 2003
GPS1_2004.txt	Daily positions GPS1 2004
GPS2_2004.txt	Daily positions GPS2 2004
GPS3a_2004.txt	Daily positions GPS3a 2004
GPS3_2004.txt	Daily positions GPS3 2004
Location_continuousGPS0304.tif	Fig. with location continuous GPS (glacier and sediments)
Readme_continuousGPS_glacier.txt	

Survey markers (glacier) folder contents

SurveyMarkers_glacier_2002to2004.txt	points surveyed with static GPS
SurveyMarkers_glacier_spring2004.txt	points surveyed with static GPS terminal area
Loc_markers_02to04_all.tif	Fig. with locations of survey markers on glacier
Loc_markers_02to04_termArea.tif	Fig. survey markers on glacier, terminal area
Loc_markers_spring04.tif	Fig. survey markers close to terminus spring 2004
Readme_SurveyMarkers_glacier.txt	

Continuous GPS (sediments) folder contents

GUS2-TK03.txt	solution for cont. GPS on sediments 2003 relative to Gustavus
WHIT-TK03.txt	solution for cont. GPS on sediments 2003 relative to Whitehorse
TK03pfiles.txt	solution for cont. GPS on sediments 2003 in ITRF2000
GUS2-TK04.txt	solution for cont. GPS on sediments 2004 relative to Gustavus
WHIT-TK04.txt	solution for cont. GPS on sediments 2004 relative to Whitehorse
TK04pfiles.txt	solution for cont. GPS on sediments 2004 in ITRF2000
Location_continuousGPS0304.tif	Fig. with location continuous GPS (glacier and sediments)
Readme_continuousGPS_sediments.txt	

Survey markers (sediments) folder contents

straindiamond_august2002.txt	GPS positions of markers in proglacial area August 2002
straindiamond_june2003.txt	GPS positions of markers in proglacial area August 2003
straindiamond_august2003.txt	GPS positions of markers in proglacial area August 2003
straindiamond_mayjune2004.txt	GPS positions of markers in proglacial area August 2004
straindiamond_august2004.txt	GPS positions of markers in proglacial area August 2004
Location_straindiamonds.tif	Figure with location and numbering of GPS positions
Readme_straindiamonds.txt	

Isotope analysis folder contents

Kuriger release06Jul2004.txt	original folder with test results of ice and water samples
Isotopes2004.txt	original file annotated
Readme_isotopes.txt	

Kinematic profiles folder contents

kinematic_bulges_june03.txt	position along the toe of the bulges June 2003
kinematic_profiles_june03.txt	4 profiles across bulges, June 2003
TakuTerminus1989.txt	Coordinates for terminus location 1989
TakuTerminus1996.txt	Coordinates for terminus location 1996
TakuTerm_june2001.txt	Coordinates for terminus location June 2001
TakuTerm_june2002.txt	Coordinates for terminus location June 2002
TakuTerm_fall2002.txt	Coordinates for terminus location fall 2002
TakuTerm_march2003.txt	Coordinates for terminus location March 2003
TakuTerm_june03_west.txt	Coordinates for terminus location June 2003
TakuTerm_june03_east.txt	Coordinates for terminus location June 2003
TakuTerm_may2004.txt	Coordinates for terminus location May 2004
taku04May_terminus.xls	
Readme_kinematic.txt	

Climate folder contents

TAKU_ablmeter_2003.txt	original data from Ablationmeter
TAKU_ablmeter_2003.xls	annotated data Ablationmeter
TAKU_abl_daily_2003.txt	daily ablation 2003
TAKU_HOBOTemp_2003.txt	temperature on Taku push moraines 2003
TAKU_HOBOTemp_2004.txt	temperature on Taku push moraines 2004
Taku_HOBOtemp_winter0304.txt	
Taku_meanTemp_2003.txt	mean daily temperature, from TAKU-HOBOTemp_2003.txt
Taku_precip_2003.xls	precipitation on Taku push moraines 2003
Taku_precip_winter0304.txt	
Juneau_meanTemp0304.txt	mean daily air temperature Juneau Airport March03-Aug04
Juneau_precip0304.txt	daily precipitation Juneau Airport March03-Aug04
mendenhall_river_discharge_0304.txt	water discharge Mendenhall River Juneau 2003/2004
Readme_climate.txt	

Photogrammetry folder contents

Final_XYZ_2002.txt	3m DEM 2002
bumpsonly_XYZ_2002.txt	3m DEM, section of Final_XYZ_2002.txt
TakuOrtho_2_2002.tif	Orthophoto 2002
Taku_2003_DTM.txt	3m DTM, Taku terminal area 2003
Taku_Fall2003_CMP.txt	3m DTM, section of Taku_2003_DTM.txt
photocontrol_points	folder with .xls files for control point coordinates
Readme_photogrammetry.txt	

Laser altimetry folder contents

1993	altimetry data 1993
1996	altimetry data 1996
1999	altimetry data 1999
2000	altimetry data 2000
2001	altimetry data 2001
Readme_laseraltimetry.txt	

Pictures folder contents

All pictures of the thesis in color, as .jpg

All figures of thesis, as .eps and .tif

Miscellaneous

manual_coordinate_systems.doc	manual for coordinate transformation
ek_master_thesis_june05.pdf	master thesis
ek_thesis_defense_june05.ppt	oral presentation thesis defense